Journal of *Marine Science and Engineering*

MDPI

Article

Pb-210 Dating of Ice Scour in the Kara Sea

Osip Kokin [1,2,*], Irina Usyagina [3], Nikita Meshcheriakov [1,3], Roman Ananiev [4], Vasiliy Arkhipov [1,2], Aino Kirillova [1], Stepan Maznev [1,2], Sergey Nikiforov [4] and Nikolay Sorokhtin [4]

[1] Geological Institute, Russian Academy of Sciences (GIN RAS), 7 Pyzhevsky per., 119017 Moscow, Russia
[2] Faculty of Geography, Lomonosov Moscow State University (MSU), GSP-1, 1 Leninskie Gory, 119991 Moscow, Russia
[3] Murmansk Marine Biological Institute, Russian Academy of Sciences (MMBI RAS), 17 Vladimirskaya St., 183010 Murmansk, Russia
[4] Shirshov Institute of Oceanology, Russian Academy of Sciences (IO RAS), 36 Nakhimovsky Prospect, 117997 Moscow, Russia
* Correspondence: osip_kokin@mail.ru

Abstract: Ice scours are formed when the keels of floating icebergs or sea ice hummocks penetrate unlithified seabed sediments. Until now, ice scours have been divided into "relict" and "modern" according to the water depth that corresponds with the possible maximum vertical dimensions of the keels of modern floating icebergs. However, this approach does not consider climatic changes at the present sea level, which affect the maximum depth of ice keels. We present an application of ^{210}Pb dating of the largest ice scour in the Baydaratskaya Bay area (Kara Sea), located at depths of about 28–32 m. Two sediment cores were studied; these were taken on 2 November 2021 from the R/V *Akademik Nikolay Strakhov* directly in the ice scour and on the "background" seabed surface, not processed via ice scouring. According to the results of ^{210}Pb dating, the studied ice scour was formed no later than the end of the Little Ice Age. Based on the extrapolation of possible sedimentation rates prior to 1917 (0.22–0.38 cm/year), the age of the ice scour is estimated to be 1810 ± 30 AD. The mean rate of ice scour filling with 70 cm thick sediments from the moment of its formation is around 0.33 cm/year.

Keywords: ice gouge; iceberg ploughmark; sediment core; bathymetry; seismic profiles; sediment accumulation rate (SAR); specific activity; radionuclides; Baydaratskaya Bay

check for updates

Citation: Kokin, O.; Usyagina, I.; Meshcheriakov, N.; Ananiev, R.; Arkhipov, V.; Kirillova, A.; Maznev, S.; Nikiforov, S.; Sorokhtin, N. Pb-210 Dating of Ice Scour in the Kara Sea. *J. Mar. Sci. Eng.* **2023**, *11*, 1404. https://doi.org/10.3390/jmse11071404

Academic Editors: George Kontakiotis, Angelos G. Maravelis, Avraam Zelilidis and Antoni Calafat

Received: 24 March 2023
Revised: 30 June 2023
Accepted: 3 July 2023
Published: 12 July 2023

Copyright: © 2023 by the authors. Licensee MDPI, Basel, Switzerland. This article is an open access article distributed under the terms and conditions of the Creative Commons Attribution (CC BY) license (https://creativecommons.org/licenses/by/4.0/).

1. Introduction

Ice scours (ice gouges, ice ploughmarks) are widespread on the bottom of high- and mid-latitude seas and big freezing lakes at different water depths up to 500 m [1–12] and occasionally up to 1200 m [13,14]. They are formed when the keels of floating icebergs or sea ice hummocks (pressure ridges) collide with unlithified seabed sediments. The study of the ice scouring process has become especially important in recent times due to climate change. Additionally, these kinds of processes are a natural risk for the development of Arctic shelf oil and gas fields and the Northern Sea Route, adversely affecting the construction and operation of structures and the movement of ships in the Barents–Kara region.

For the purposes of marine engineering, it is important to understand in which areas ice scouring can still occur, and in which areas ice scours on the seabed are relicts. During the construction of submarine structures such as pipelines, it is also important to understand under what conditions (sea level, climate) the depth of penetration of ice keels into the bottom sediments is observed. To answer these questions, the dating of ice scours, which to our knowledge has not yet been achieved, could help. Only the dating of completely buried iceberg scour relicts (with the age around 31 kyr cal BP) in the subtropical North Atlantic is known [15]. Their age has been estimated based on radiocarbon dating of sediment samples above and below the iceberg scour surface.

To estimate the age of ice scours, the water depth at which they are observed is now the most widely used [3,7,8,12,13]. According to this, ice scours are divided into "relict" (formed at another relative sea level other than the present) and "modern" (formed at the present sea level). Ice scour relicts are located at a water depth significantly exceeding the possible maximum vertical dimensions of the keels of modern floating icebergs. The threshold between modern iceberg scours and iceberg scour relicts varies widely depending on the area and in the range of 40 to 550 m [3,4,7,8]. However, this approach does not take into account climatic changes at the present sea level which affect the maximum depth of ice keels and, accordingly, the depth of the seabed at which the ice scours were formed and located in the corresponding climatic period.

Another attempt to date ice scours is based on the identification of newly formed ice gouges because of a comparison of multitemporal bottom surveys carried out during monitoring [16,17]. This approach has its disadvantages: it requires many years of observations, does not consider the extreme sizes of ice keels and is limited in space.

The method of marine sediment dating using non-equilibrium lead ($^{210}Pb_{ex}$), which is widely used to determine sedimentation rates over the past 100–120 years, could expand the possibilities for estimating the age of ice scours [18]. However, we are not aware of any attempts to date ice scours based on measurements of the specific activity of the natural radionuclide ^{210}Pb. In this regard, the main objective of the present study is to show the possibility of the well-established ^{210}Pb geochronology approach to ice scour dating.

2. Study Area

The study area is located in front of the entrance to Baydaratskaya Bay in the southwestern semi-enclosed part of the Kara Sea. The ice scours of the bay are the most studied in the entire Kara Sea [19]. They began to be investigated in 1988 as part of the design of a submarine gas pipeline crossing the bay. The largest ice scour known in this area was chosen for dating using the non-equilibrium lead method.

The studied ice scour is located at depths of about 28–32 m (Figure 1), which are close to the estimates of the maximum keel depths of sea ice features (stamukhi and hummocks) in the Kara Sea—no more than 28 m [20]. The maximum keel depth of modern icebergs in the Kara Sea is estimated to be no more than 180–200 m and the average is about 50 m [21]. There are known facts of iceberg penetration into Baydaratskaya Bay with depths of less than 20 m during periods of minimal ice cover in the Kara Sea in 1932 and 2007 [22].

From the point of view of the geomorphological structure of the bottom, the study area is located on a gently sloping coastal plain which extends to depths of 50–60 m and is bounded from the open sea side by a tectonic scarp [23]. By the beginning of the postglacial transgression, this plain was in subaerial conditions. During transgression, its surface from the scarp crest to the modern coastline was reworked by wave processes. It is assumed that about 10 kyr BP, there was a period of relative sea level stabilization at the modern sea depth of 32–34 m [23].

The Baydaratskaya Bay area is characterized by low average annual temperatures (from −7 to −10 °C) and a relatively short ice-free period (1–4 months a year) [19]. Over the past 50 years, there has been a tendency for the ice-free period to increase [24]. The sea ice of Baydaratskaya Bay consists of fast ice along the coast and drift ice offshore [25]. The maximum fast ice rim position generally varies in the range of sea depths of 10–20 m [26].

The wind and currents are the driving forces of ice drift. During the winter season, southerly and southwesterly winds prevail in the Baydaratskaya Bay area [25]. The currents here are associated with semi-diurnal tides and they are practically reversive and aligned along the axis of the bay. The maximum speed of the tidal current during the tidal cycle is 0.5 m/s, while the measured maximum current speed is 1 m/s [25]. Sea level fluctuations are associated with tides (up to 1.1 m) and storm surges (up to 2 m).

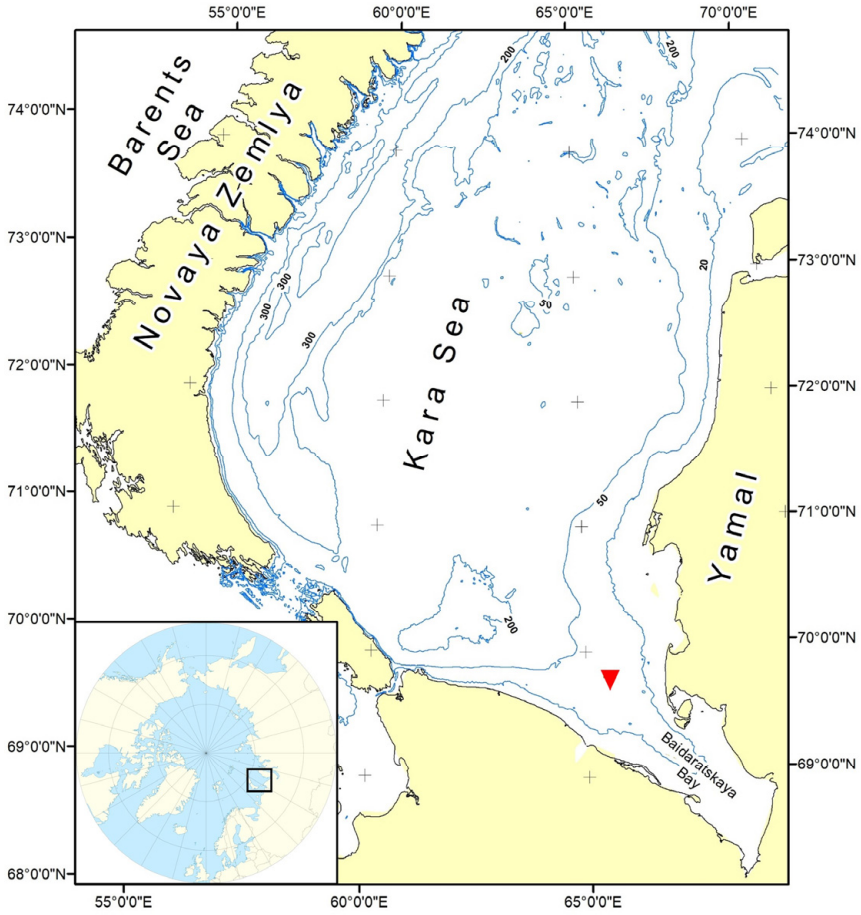

Figure 1. The overview map. The red triangle indicates the location of the studied area in the Kara Sea. The 20, 50, 200 and 300 m depths are indicated by the contour lines. The inset map shows the location of the Kara Sea.

Ice scours are widespread in Baydaratskaya Bay to depths of more than 12 m and can be up to 2 m deep, 50 m wide and several kilometers long [5]. In shallower areas, ice scouring processes are also active, but wind waves destroy their evidence during strong summer and autumn storms. The most intensive and deep ice scours occur at the range of depths from 16 to 19 m next to the Yamal coast fast ice rim, where ice hummocks continue during the whole of the cold season [5]. The predominant orientation of the ice scours corresponds to the direction of reverse tidal currents along the axis of the bay.

Sedimentation rates in the Kara Sea are presented mainly as average values for the thickness of the Holocene deposits [27]. More precisely, the sedimentation rate was determined using the method of accelerator mass spectrometry (AMS ^{14}C) using carbonate shells of mollusks and foraminifers only for a few single horizons of the sedimentary section [28,29].

Sedimentation rates determined by ^{210}Pb in the Kara Sea are presented in [30–32]. Fourteen cores of sediments up to 50 cm long were studied in key areas of the bottom deposit accumulation in the Kara Sea: the estuaries of the Ob and Yenisei, the East Novaya Zemlya Trench, the Voronin Trench and also in one of the northern bays of the Novaya Zemlya (Sedov Bay) [33]. However, all of them differ from Baydaratskaya Bay in terms of sedimentation conditions. The sedimentation rates were determined by measuring the specific activity of the natural ^{210}Pb and technogenic ^{137}Cs radionuclides. A close relationship was shown between the sedimentation rates and types of seabed sediments. The highest sedimentation rates are typical of terrigenous–estuary sediments, which are

divided into traction sediments with sedimentation rates of 0.4–0.7 cm/year and sediments of "silt banks" with sedimentation rates of 0.7–1.0 cm/year [33].

3. Materials and Methods

The present study is based on the results of the seabed topography and sediment investigations of the Kara Sea by the Shirshov Institute of Oceanology RAS cruise 52 of the R/V *Akademik Nikolai Strakhov* (ANS) [34], which took place from 15 October to 10 November 2021. During the cruise, complex geological and geophysical, geomorphological and hydrophysical studies were carried out. One of the objectives of the cruise was a detailed study of the large ice scours in the Kara Sea.

3.1. Multibeam Echo Sounding

Multibeam echo sounding was carried out for the seabed topography mapping to obtain information about the morphology, morphometry and configuration of the ice scour. For this, a multibeam echo sounding system of the R/V *Akademik Nikolaj Strakhov* was used. It consists of a Reson 100 kHz SeaBat 8111, an Applanix POSMV integrating motion sensor and gyrocompass data. The multibeam transducers are installed in a hull-mounted gondola. The swath-bathymetric data were collected and processed using the PDS2000 software from Teledyne. The processed data were gridded at cell sizes of 4×4 m, and visualizations were carried out using PDS2000, ArcGIS and QGIS software. The survey area consisted of a series of single survey lines with a total length of about 35 km along and across the studied ice scour (Figure 2).

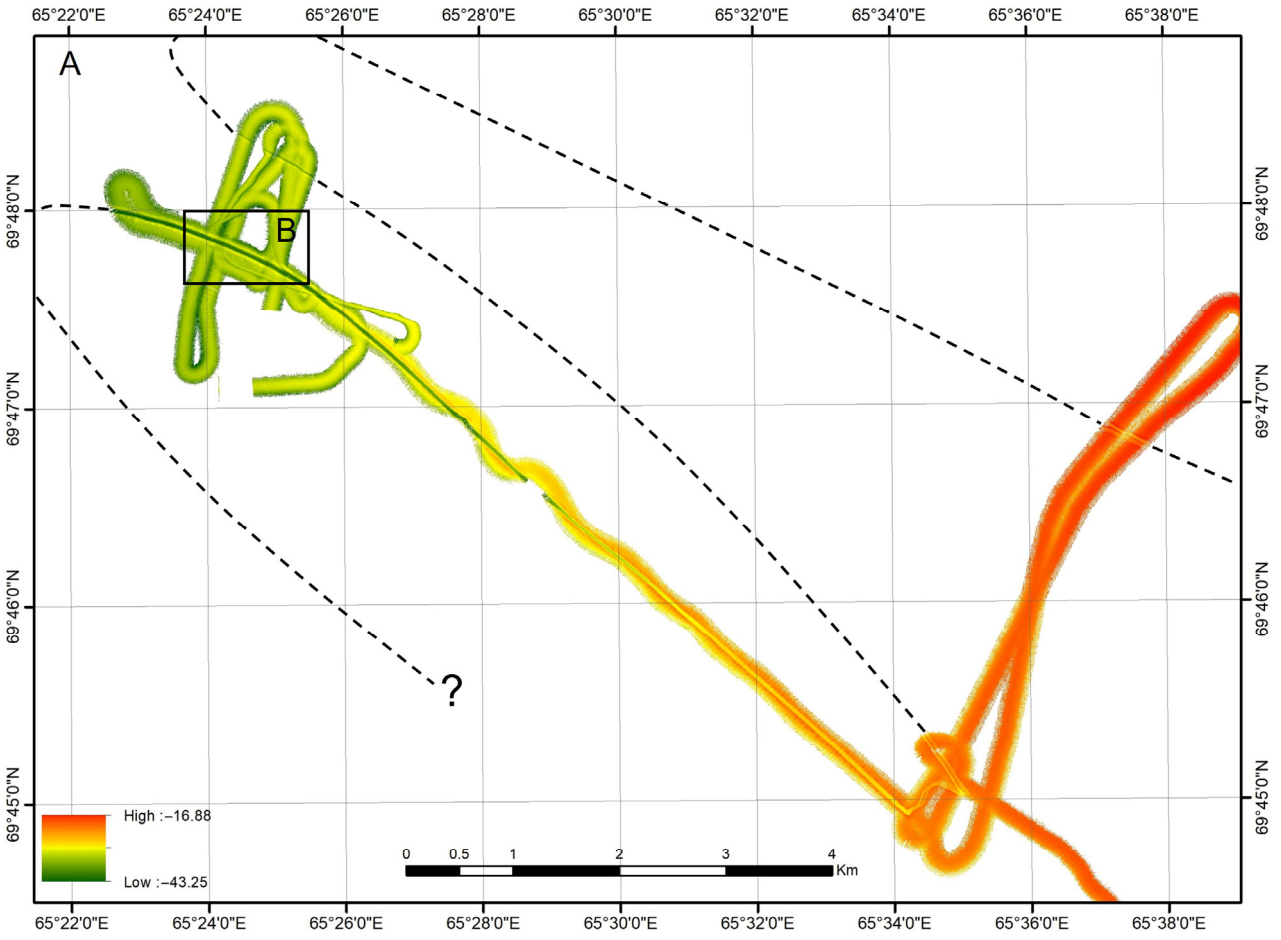

Figure 2. *Cont.*

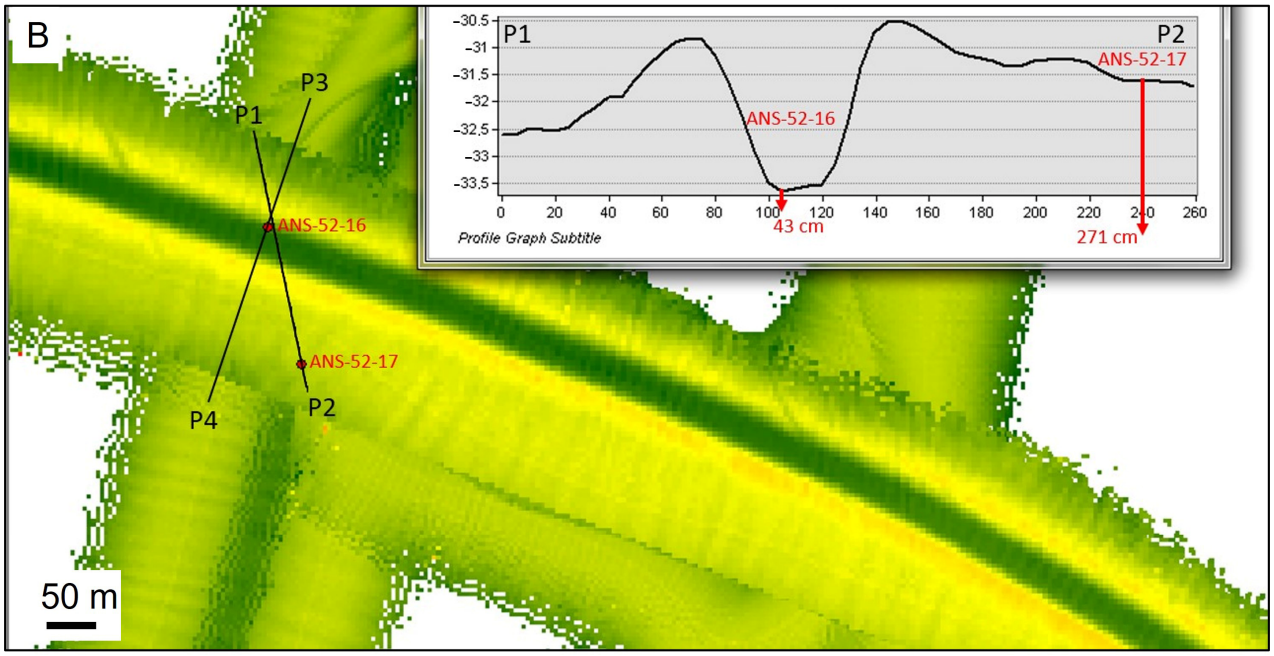

Figure 2. (**A**) Seabed topography in the area of the studied ice scour and estimated ice scour configuration outside of the survey area (dashed black line); (**B**) detailed seabed topography near the sampling site with a bathymetric profile P1–P2 drawn through the core sampling points ANS-52-16 ("in a gouge", sea depth 33.6 m) and ANS-52-17 ("background", sea depth 31.6 m). The black lines show the location of the bathymetric profile P1–P2 and the seismic profile P3–P4 (Figure 3). The red arrows on the bathymetric profile P1–P2 show the length of the sampled sediment cores.

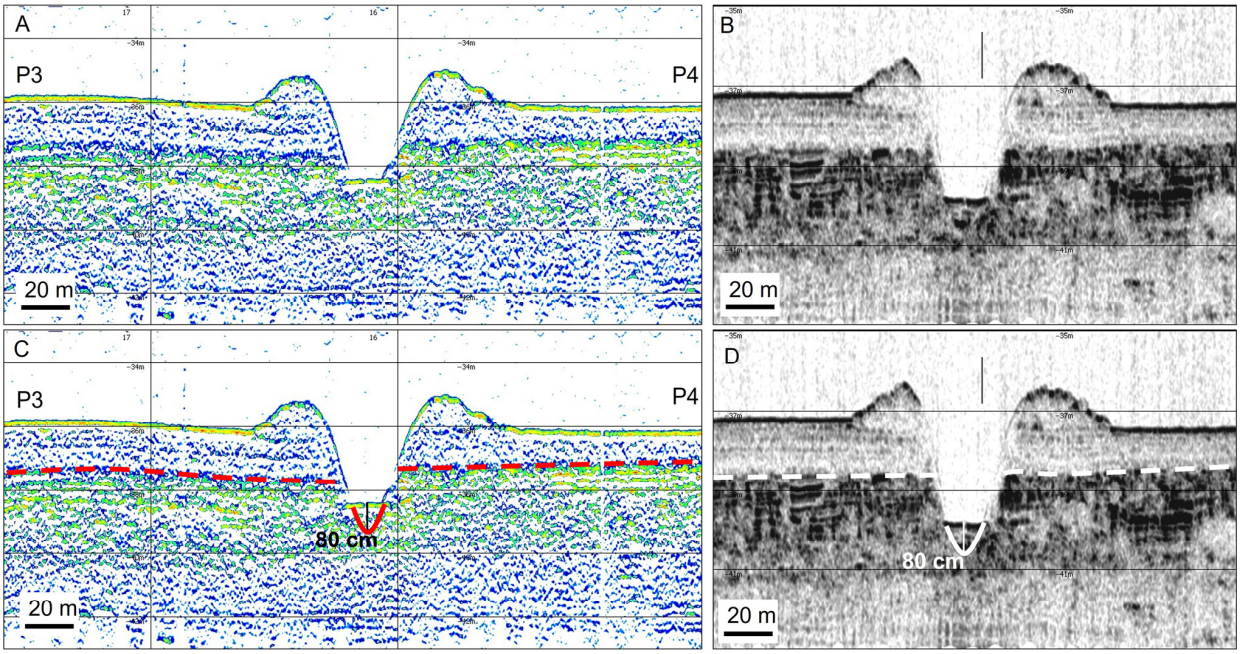

Figure 3. The seismic profiles crossing the ice scour in the core sampling area. (**A**) The seismic profile P3–P4 (the location is indicated in Figure 2B); (**B**) the seismic profile 400 m to SE from P3–P4; (**C**) the seismic profile P3–P4 with interpretation; (**D**) the seismic profile 400 m to SE from P3–P4 with interpretation. The solid line (red and white) highlights the deposits that filled the ice scour after the last one was formed, with indication of the measured thickness. The dotted line (red and white) shows the boundary between Late Holocene (above) and Late Pleistocene (below) deposits.

3.2. Seismic Profiling

Seismic profiling was carried out to assess the thickness of the deposits filling the ice scour and to obtain information about the structure of the sedimentary strata in which the ice scour was formed. For this, an EdgeTech 3300 high-resolution seismic profiler (sub-bottom chirp) and the seismoacoustic complex Geont-shelf with a sparker source were used. The sub-bottom transducers were installed in a hull-mounted gondola. In addition, the high-resolution parametric sub-bottom profiler SES-2000 Standard with frequencies of 8–10 kHz was installed on a pole on the starboard. The studies were carried out using a single-channel seismic streamer.

Seismic profiling was carried out along all multibeam echo sounding lines with a total length of about 35 km, but in this work, only seismic profiles located near the sampling site of the sediment core were used (Figure 2). In addition, profiles obtained near the sampling site during previous cruises were involved in the analysis.

3.3. Sediment Cores

In the present study, two sediment cores (ANS-52-16 and ANS-52-17) were studied (Table 1). They were taken on 2 November 2021 (2021.8 AD) using a 147 mm gravity corer from R/V *Akademik Nikolaj Strakhov* near the entrance of Baydaratskaya Bay in the Kara Sea (Figure 1). The first core (ANS-52-16, length 43 cm) was taken directly in the ice scour at a water depth of 33.6 m; the second one (ANS-52-17, length 271 cm) was taken at a depth of 31.6 m from the "background" seabed surface south of the ice scour, not reworked by ice ploughing (Figure 2). In the present study, the first core is called "ice scour", and the second is called "background". The distance between cores is about 140 m.

Table 1. Sediment cores studied in the present study.

Sediment Core	Position	Sampler	Latitude (°N)	Longitude (°E)	Cruise	Water Depth, m	Length, cm
ANS-52-16	Ice scour	147 mm gravity corer	69.797683	65.40115	ANS-52	33.6	43
ANS-52-17	Background	147 mm gravity corer	69.796467	65.40185	ANS-52	31.6	271

Since coring from a relatively narrow ice scour constitutes a complex task, the results of the core analysis from the "background" seabed surface that had not been reworked by ice ploughing should confirm or disprove that the first core was indeed taken from the ice scour. This approach is based on the fact that the sedimentation conditions within and outside of the ice scour should be different and therefore the results from the analyses should show different patterns in these cores.

The following technique was used to increase the probability of core sampling directly from the ice scour. The vessel approached the ice scour with a predetermined spatial configuration and a preselected sampling site (according to multibeam echo sounding and seismic profiling) at an angle that provided greater distance during the ice scour crossing. During the vessel drift, the gravity corer was hung out at a given horizon (approximately 20 m from the bottom); then, when the vessel was in position at the planned sampling point, on command from the Captain's Bridge, the gravity corer was released on the winch freewheel. At the moment when the gravity corer touched the seabed (determined by the sagging of the cable) the precise coordinates of the sampling point were recorded.

After the cores were recovered onboard the vessel, they were photographed and their lithology was visually described. For further laboratory analysis of the ice scour dating, the cores were packed into plastic cable channels 50 cm long, either completely (43 cm of "ice scour" core) or only the upper part of the core (50 cm of "background" core). Cores packed in cable channels were subjected to quick freezing (−18 °C) onboard the vessel and sent frozen to the laboratory of the Murmansk Marine Biological Institute of the Russian Academy of Sciences.

The sampling for laboratory analysis of only the upper 50 cm of cores is explained by the fact that the expected age of deposits below 50 cm should be significantly more than 100–120 years, which exceeds the dating capabilities of the non-equilibrium lead method.

3.4. Grain Size Analysis

Grain size analysis was carried out in the laboratory of Murmansk Marine Biological Institute with wet samples using the wet sieve and decantation methods, which are considered to be the most accurate for fine sediments, as they are based on the hydraulic settling of particles according to the Stokes formula [35]. The accuracy of settling in each stage was controlled by a microscope. The classification of M.V. Klenova was used to interpret the types of bottom sediments based on the results of grain size analysis [36].

The sampled cores were divided into layers of 1–5 cm for detailed studies. A total of 44 samples were analyzed: 20 in the "ice scour" core (0–30 cm) and 22 in the "background" core (0–50 cm). Grain size is given in weight percent of the total sample. Moisture content was determined for each sample together with grain size analysis.

3.5. Radiometric Measurements ^{210}Pb, ^{226}Ra, ^{137}Cs and ^{7}Be

The measurement of specific activity of ^{210}Pb, ^{226}Ra, ^{137}Cs and ^{7}Be radionuclides was carried out in the laboratory of the Murmansk Marine Biological Institute using a multichannel gamma-ray spectrometer for measuring X-ray and gamma radiation (Canberra Semiconductors NV, Olen, Belgium) with lead screen protection of the HPGe detector Ekran-2P manufactured by Aspect (Dubna, Russia). For the recording part, a BE5030 broadband detector made of ultrapure germanium planar type with a thin "carbon epoxy" entrance window (0.6 mm wide) and a crystal (diameter of 80 mm, an area of 5000 mm^2 and a thickness of 30.5 mm) was used. It records gamma quanta with energy from 3 keV to 3 MeV. The energy resolution along the 1332 keV ^{60}Co line is no less than 2.2 keV; along the ^{57}Co 122 keV isotope line, it is no less than 0.75 keV, and along the ^{55}Fe isotope line, it is no less than 0.5 keV. Spectral information was collected using a DSA-1000 pulse analyzer (Canberra Industries, Inc., Loches, France) with a resolution of 16K channels, corresponding to modern digital signal processing technology. Spectra processing took place and radionuclides were identified using Genie-2000 software (version 3.3).

The sampled cores were divided into layers of 1–2 cm for detailed studies. A total of 56 samples were analyzed: 36 in the "ice scour" core (0–43 cm) and 20 in the "background" core (0–25.5 cm). All sediment samples were dried before measurement, homogenized and left for 30 days in hermetically sealed vessels to ensure secular equilibrium between ^{226}Ra and ^{222}Rn, as well as ^{214}Pb and ^{214}Bi [37,38]. The measurement of each layer was carried out in the same vessels after the onset of equilibrium between the indicated radionuclides. The measurement time was 85,000 s, which gave an error calculation of 5–15% in the upper layers of the cores. The activity of the supported ^{210}Pb determined from the main ^{226}Ra lines was subtracted to determine the excess ^{210}Pb activity ($^{210}Pb_{ex}$) from the total ^{210}Pb specific activity measured from its γ-line (46.5 keV). The quantification of ^{226}Ra was carried out by ^{214}Pb (295.2 keV and 351.9 keV) and ^{214}Bi (1120 keV). The $^{210}Pb_{ex}$ activity was corrected for the date of core collection (2021.8 AD) and the results are given on a dry weight basis, corrected for self-absorption and sample geometry [39]. The short-lived radionuclide ^{7}Be was measured in the uppermost layer to confirm that the surface layer was sampled correctly.

A quality check of the gamma spectrometer efficiency was carried out regularly with the help of two volumetric activity measures issued for special purposes by the D.I. Mendeleyev Institute for Metrology (VNIIM). The density of the the volumetric activity measure fillers was 1.01 g/cm^3. The activity of ^{210}Pb deposited on the filler was 1.64 kBq; the activity of ^{137}Cs was 1.4 kBq. The specific activity of ^{226}Ra was determined via the source of ^{152}Eu, and the activity of ^{152}Eu in the source was 3.78 kBq.

3.6. Calculation of the Calendar Age and the Sediment Accumulation Rates Based on the Results of Radiometric Measurements

^{210}Pb dating of marine sediments is an accessible and widely used method used to estimate the rates of modern sedimentation in the Arctic seas [31–33,40–44]. The simultaneous determination of natural ^{210}Pb and ^{226}Ra and technogenic ^{137}Cs in a sample became possible after the advent of modern gamma spectrometers for measuring X-ray and gamma radiation and detecting gamma rays with energies from 3 keV to 3 MeV. This significantly reduced the analysis time and made it possible to use the measured material for other studies.

The natural radionuclide ^{210}Pb has a half-life ($T_{1/2}$) of 22.3 years and is a member of the ^{226}Ra decay chain ($T_{1/2}$ = 1600 years) that is produced via the successive decay of the parent isotope ^{238}U. ^{210}Pb in marine sediments consists of supported ^{210}Pb, which is continuously formed and, presumably, is in secular equilibrium with its initial radionuclide ^{226}Ra and excess ^{210}Pb. The last one enters the surface of water bodies and the surrounding drainage area, and then makes its way into the bottom sediments as a result of atmospheric deposition. The excess ^{210}Pb is determined by subtracting the supported ^{226}Ra activity from the total ^{210}Pb activity and is used to determine the age of sediments in a sedimentation basin. However, compared to other isotopes used for geochronology, such as ^{14}C ($T_{1/2}$ = 5730 years), excess ^{210}Pb can only be used to date the age of recent deposits formed within the last 100–120 years [45,46].

Many studies have shown that the analysis of data and interpretation of the results obtained by dating via excess ^{210}Pb are often associated with certain assumptions and limitations [47–50]. The age of the sediments is calculated using an exponential equation that describes the decrease in the total specific activity of ^{210}Pb with depth, only if the flow of excess ^{210}Pb to the sediment surface is constant and there are no processes leading to its mixing or redistribution (constant sedimentation) [49]. Often, these conditions are not met and significant fluctuations in the ^{210}Pb content can be found in the vertical profiles of the deposits. To avoid questionable or inaccurate interpretations of ^{210}Pb profiles, the chronology of ^{210}Pb should always be confirmed using independent time markers (e.g., ^{137}Cs) or any other available geochemical indicators [49,51].

The calendar age and the sediment accumulation rates of layers in the studied sediment cores were calculated using the constant flux (CF) model based on the data of the excess ^{210}Pb activity [49]. The CF model makes it possible to consider the uneven supply of ^{210}Pb with the flow of sediment mass to the seabed surface. Layers lying below the accepted equilibrium boundary are not considered during sediment age calculations. The formulae used for the calculation are presented in the Supplementary Materials.

The independent verification of chronology is essential to ensure a high level of confidence in the results. Therefore, the known independent key date method was used. Artificial radionuclides make it possible to determine several key dates in the last 70 years. The ^{137}Cs chronostratigraphic marker is widely used to date sediment cores in the Arctic, as the radioactive fallout from atmospheric nuclear weapon testing was global. Thus, the presence of a concentration peak in most cases makes it possible to determine the depth of contamination with a known event date [52]. The calculated ages of studied sedimentary layers are verified using the results of measuring the specific activity of the technogenic radionuclide ^{137}Cs, especially since the nuclear tests were carried out relatively close to the study area—on the Novaya Zemlya archipelago.

3.7. Estimation of Ice Scour Age

Ice scour age estimation is based on the fact that the sedimentation in it commences immediately after its formation as a result of the impact of drifting ice on the seabed. Therefore, if we determine the age of the lower sediment layers filling the ice scour, we can determine the age of the ice scour itself. The extrapolation of the sedimentation rate, determined from ^{210}Pb in the upper layers, was used to estimate the age of the lower

sediment layer of the ice scour in case it exceeded the capabilities of the ^{210}Pb dating method (100–120 years).

4. Results

4.1. Ice Scour Structure

At depths of 28–32 m, a multibeam echo sounder mapped an almost rectilinear segment 10.8 km long of the ice scour (in front of the Baydaratskaya Bay entrance, Figure 2), oriented NW–SE at an angle to the isobaths and located almost on the continuation of the bay axis (Figure 1). The maximum depth of the ice scour cutting into the background surface was 3.2 m, and the maximum width did not exceed 35 m. Side berms up to 1.5 m high could be traced almost along the entire ice scour.

The ice scour made a U-turn of almost 180 degrees, at the SE end of the segment, and after which the survey was interrupted, making it impossible to trace the further configuration of the ice scour. However, on the tacks transverse to the main ice scour, the minor fragments of some ice scours were recorded, which presumably could be a continuation of the main ice scour. In this case, the ice scour had a serpentine-shaped plan configuration, changing its direction 2–3 times and reaching a length of at least 30–35 km (dashed black line in Figure 2A). Such a configuration indicates that the main driving force in the formation of the ice scour was reverse tidal currents. At the SE end of the segment where the U-turn occurs, the ice scour becomes double.

Core sampling was carried out in the NW part of the studied segment of the ice scour. Here, it had an asymmetric structure—the southern side was 0.5–1.0 m higher than the northern one (Figure 2B). At the core sampling site, the apparent depth of the ice scour cutting into the background seabed surface was about 2.4 m. According to seismic profiles, the thickness of sediments filling the ice scour was estimated at about 0.6–0.8 m (Figure 3). Thus, the initial depth of the ice scour cutting into the background seabed surface at this location could be up to 3.2 m.

Two sediment units are clearly visible on the seismic profiles crossing the ice scour in the core sampling area (Figure 3). The upper unit, 1.5–2 m thick, covers the underlying layers like a mantle and is displayed on the seismic profiles mainly as an acoustically transparent stratum, which is due to its water saturation and the relatively fine composition of sedimentary material. The almost-complete absence of acoustically pronounced boundaries in this unit may indicate that it was formed under the conditions of a stable water basin, i.e., without significant changes in sedimentation. This allowed us to assume their formation over the past 5–6 kyr BP, when the sea level became close to modern. Thus, we interpreted the age of the upper unit as Late Holocene.

The lower unit has a "chaotic" wavefield pattern, which is characterized by numerous short sub-horizontal and inclined axes of commonality (Figure 3). These deposits are characterized by a complex facies composition laterally and in depth. They are represented by lithological differences, from sands and sandy loams to clayey silts. We interpreted the age of the lower unit as Late Pleistocene. Thus, as can be seen in the seismic profiles (Figure 3), the ice scour completely cuts through Late Holocene deposits and cuts into Late Pleistocene deposits by 1.5–2 m (Figure 3).

4.2. Sediment Grain Size Distribution

Grain size analyses show that the sediments of both cores are composed exclusively of clayey silt. The pelite content (<0.01 mm) varies from 52.9 to 68.4% in the "ice scour" core, silt content (0.05–0.01 mm) ranges from 23.4 to 29.5% and heterogeneous sand (1–0.05 mm) is from 4.2 to 16.4% (Table 2). Some layers (1–2 and 15–27 cm) contain gravel grains. The highest content of fine gravel inclusions occurs in the upper part of the core (1–2 cm).

Table 2. Grain size composition and natural moisture content (W) of the "ice scour" core sediments (ANS-52-16).

Layer, cm	Thickness, cm	>1	1–0.5	0.5–0.25	0.25–0.1	0.1–0.05	0.05–0.01	<0.01	W, %
0–1	1	0	0	2.1	4.2	10.1	26.4	57.2	130
1–2	1	12.5	0.4	0.4	4.7	5.7	23.4	52.9	90
2–3	1	0	0	0.5	2.8	3.7	26.2	66.8	122
3–4	1	0	0	1.0	4.0	6.5	29.5	59.0	101
4–5	1	0	0	0	3.3	3.7	28.6	64.4	94
5–6	1	0	0	0.5	3.75	7.5	29.25	59.0	94
6–7	1	0	0	0.3	3.2	6.3	28.4	61.8	90
7–8	1	0	0	0	3.8	6.6	28.4	61.2	94
8–9	1	0	0	0	1.3	3.7	28.0	67.0	94
9–10	1	0	0	0	1.7	3.0	26.9	68.4	90
10–11	1	0	0	0	1.6	2.6	27.9	67.9	94
11–12	1	0	0	0	2.0	3.5	27.3	67.2	98
12–15	3	0	0	1.0	2.8	4.9	25.4	65.9	86
15–17	2	0.5	0.2	0.8	4.4	3.9	33.8	56.4	81
17–19	2	0.2	0.2	0.7	3.0	2.2	33.0	60.7	69
19–21	2	0	0	0.8	3.1	3.1	30.1	62.9	67
21–23	2	0.2	0.2	0.8	3.6	3.1	26.5	65.6	63
23–25	2	0	0	0.6	2.9	3.0	25.5	68.0	69
25–27	2	0.1	0.1	0.8	3.8	3.8	26.9	64.5	67
27–30	3	0	0	0.4	2.7	5.2	28.0	62.7	71

In the "background" core, the pelite content (<0.01 mm) varies from 56.6 to 72.7%, silt content (0.05–0.01 mm) ranges from 27.1 to 39.4% and the inclusion of heterogeneous sand and gravel is not significant (Table 3). Thus, the concentration of the coarse fraction in the sediments accumulated inside the ice scour is higher than in the sediments outside it, which is the main difference in the grain size composition of the studied cores. The natural moisture content of sediments (W) decreases from the upper layers to the lower ones in both cores. However, it is generally higher in the "ice scour" core (from 130 to 67%; Table 2) than in the "background" core (from 77 to 48%; Table 3).

Table 3. Grain size composition and natural moisture content (W) of the "background" core sediments (ANS-52-17).

Layer, cm	Thickness, cm	>1	1–0.5	0.5–0.25	0.25–0.1	0.1–0.05	0.05–0.01	<0.01	W, %
0–2	2	0	0	0	0	1.2	36.3	62.5	77
2–5	3	0	0	0	0	1.9	34.5	63.5	68
5–8	3	0	0	0.3	2.3	3.5	30.5	63.4	71
8–11	3	0.4	0.1	0.4	2.5	4.0	36.0	56.6	69
11–15	4	0	0	0	0.8	1.7	32.7	64.8	70
15–16	1	3.8	0	0	0	1.3	27.0	67.9	72
16–17	1	0	0	0	1.0	1.5	30.6	66.9	72
17–18	1	0	0	0	0	1.1	27.1	71.8	65
18–19	1	0	0	0	1.0	2.1	28.1	68.9	69
19–20	1	0	0	0	0.9	2.1	30.0	67.0	67
20–21	1	0	0	0	0	1.9	31.8	64.3	65
21–22	1	0	0	0	0.8	1.7	33.3	64.2	66
22–23	1	0	0	0	0	1.5	31.0	67.5	72
23–24	1	0	0	0	0	0.7	27.6	71.7	67
24–25	1	0	0	0	0	1.4	26.2	72.4	71
25–26	1	0	0	0	0.5	1.5	23.5	74.5	68
26–27	1	0	0	0	0.9	1.9	24.5	72.7	72
27–30	3	0	0	0	1.3	4.0	38.7	55.8	69
30–35	5	0	0	0.1	1.2	2.2	37.5	59.0	48
35–40	5	0	0	0.3	2.0	2.3	39.4	56.0	55
40–45	5	0	0	0.3	1.5	2.3	36.9	59.0	55
45–50	5	0.6	0.2	0.2	1.7	2.4	36.7	58.2	63

4.3. Distribution of ^{210}Pb and ^{137}Cs in Sediments of the Cores

The specific activity of ^{210}Pb reaches a maximum value of 108 Bq/kg in the upper part of the "ice scour" core sediments (Table 4). It decreases to 48–55.9 Bq/kg in the lower

layers (38–43 cm) without any significant outliers. The ^{226}Ra content varies from 14.7 to 45.7 Bq/kg throughout the sediment core, with an average value of 28.6 Bq/kg. Equilibrium with the initial radionuclide ^{226}Ra at the layer of 42–43 cm was not revealed in the "ice scour" core, but there was a tendency to approach it. The technogenic radionuclide ^{137}Cs was determined in most layers. The values ranged from less than the minimum detectable activity (<MDA) to 47.3 Bq/kg. The MDA for ^{137}Cs was 0.2 Bq/kg. The radionuclide was not found in sediment layers below 36 cm (Table 4). In the uppermost layer of the "ice scour" core (0–1 cm), short-lived radionuclide ^{7}Be was found with specific activity of 18.4 ± 8.3 Bq/kg, which confirms that the surface layer was sampled correctly.

Table 4. The results of measurements of the specific activity of short-lived radionuclides and the calculation of excess ^{210}Pb (C_i) in the "ice scour" core (ANS-52-16), Bq/kg.

Layer, cm	Thickness, cm	^{137}Cs	U [1] (^{137}Cs)	^{210}Pb	U [1] (^{210}Pb)	^{226}Ra	U [1] (^{226}Ra)	C_i	U [1] (C_i)
0–1	1	6.0	2.4	93.7	9.2	22.1	5.6	71.6	10.8
1–2	1	9.3	0.4	74.8	3.0	24.2	2.7	50.6	4.0
2–3	1	10.3	0.6	107.0	4.9	24.1	5.4	82.9	7.3
3–4	1	11.3	0.8	90.7	5.4	31.3	3.8	59.4	6.6
4–5	1	10.9	0.8	73.1	5.4	28.0	3.7	45.1	6.5
5–6	1	11.6	0.7	78.9	5.1	30.0	3.6	48.9	6.2
6–7	1	9.1	0.8	73.0	5.6	17.7	3.8	55.3	6.8
7–8	1	10.6	0.8	87.7	6.0	35.4	4.3	52.3	7.4
8–9	1	12.6	0.8	92.7	5.4	34.9	4.0	57.8	6.7
9–10	1	13.7	0.9	108.0	6.3	43.2	4.6	64.8	7.8
10–11	1	14.9	0.9	102.0	5.9	39.5	4.6	62.5	7.5
11–12	1	12.1	0.5	82.4	4.0	45.7	4.3	36.7	5.9
12–13	1	11.8	0.9	83.9	6.2	41.9	4.6	42.0	7.7
13–14	1	9.4	1.4	83.8	10.3	25.5	5.0	58.3	11.4
14–15	1	13.6	0.9	72.5	6.4	31.0	4.3	41.5	7.7
15–16	1	15.3	2.2	83.0	14.7	20.8	5.9	62.2	15.8
16–17	1	17	1.1	92.3	8.2	23.2	4.1	69.1	9.2
17–18	1	17.4	1.8	89.4	12.1	26.1	5.3	63.3	13.2
18–19	1	13.4	0.9	84.9	6.7	27.9	3.6	57.0	7.6
19–20	1	11.9	1.8	66.1	12.7	22.7	4.6	43.4	13.5
20–21	1	2.9	0.6	71.5	5.5	24.4	3.5	47.1	6.5
21–22	1	<MDA	-	66.7	4.7	25.8	3.9	40.9	6.1
22–23	1	<MDA	-	57.3	5.9	22.4	4.8	34.9	7.6
23–24	1	<MDA	-	47.3	4.9	17.4	4.5	29.9	6.7
24–25	1	<MDA	-	43.7	4.9	14.4	3.5	29.3	6.0
25–26	1	<MDA	-	40.0	4.8	17.9	3.3	22.1	5.8
26–27	1	8.1	0.4	45.5	2.9	21.0	3.4	24.5	4.5
27–28	1	<MDA	-	56.8	5.9	26.4	4.2	30.4	7.2
28–30	2	<MDA	-	52.1	4.9	26.6	4.1	25.5	6.4
30–32	2	47.3	0.9	56.1	3.6	22.5	2.4	33.6	4.3
32–34	2	2.4	0.6	59.3	4.1	24.2	2.7	35.1	4.9
34–36	2	2.3	0.4	41.7	3.5	19.3	2.7	22.4	4.4
36–38	2	<MDA	-	43.9	6.3	23.7	3.3	20.2	7.1
38–40	2	<MDA	-	48.0	4.8	20.0	2.1	28.0	5.2
40–42	2	<MDA	-	55.9	4.8	25.0	3.9	30.9	6.2
42–43	1	<MDA	-	52.5	4.0	24.5	4.4	28.0	5.9

[1] U—standard uncertainty.

In the "background" core sediments, the highest specific activity of ^{210}Pb is in the upper part, reaching 60 Bq/kg (Table 5). It decreases to 26.7–33.4 Bq/kg in the lower layers (17.5–25.5 cm). The ^{226}Ra content varies from 20.5 to 30.4 Bq/kg throughout the sediment core, with an average value of 23.5 Bq/g. The equilibrium of ^{210}Pb (32.9 Bq/kg) with the initial radionuclide ^{226}Ra (31.1 Bq/kg) is observed in the layer of 19.5–21.5 cm. The underlying two layers (21.5–25.5 cm) show C_i values (Bq/kg) of less than 1.0, considering the standard uncertainty. This allows us to take 19.5 cm as the equilibrium boundary for ^{210}Pb and ^{226}Ra. The layers below the accepted equilibrium boundary were not considered during sediment age calculations [49]. The ^{137}Cs specific activity in all layers was below the MDA, except for layers of 1–2 cm and 10–11 cm (Table 5). The distribution of ^{210}Pb

excess in both sediment cores demonstrates the same pattern: an exponential decrease in depth with some fluctuations, whereby the peaks of which are correlated between the cores (Figure 4).

Table 5. Results of measurements of the specific activity of short-lived radionuclides and calculation of excess ^{210}Pb (C_i) in the "background" core (ANS-52-17), Bq/kg.

Layer, cm	Thickness, cm	^{137}Cs	U [1] (^{137}Cs)	^{210}Pb	U [1] (^{210}Pb)	^{226}Ra	U [1] (^{226}Ra)	C_i	U [1] (C_i)
0–1	1	<MDA	-	60.0	0.8	26.2	6.0	33.8	6.1
1–2	1	2.2	0.3	50.1	1.5	24.2	3.4	25.9	3.7
2–3	1	<MDA	-	36.0	5.0	25.3	4.9	10.7	7.0
3–4	1	<MDA	-	55.4	6.0	20.7	4.9	34.7	7.7
4–5	1	<MDA	-	35.5	3.6	16.1	4.3	19.4	5.6
5–6	1	<MDA	-	49.9	6.6	28.0	3.3	21.9	7.4
6–7	1	<MDA	-	49.3	4.6	28.0	5.2	21.3	6.9
7–8	1	<MDA	-	27.6	6.1	22.3	4.2	5.3	7.4
8–9	1	<MDA	-	45.3	3.6	21.5	5.0	23.8	6.2
9–10	1	<MDA	-	54.6	6.6	23.7	4.0	30.9	7.7
10–11	1	1.1	0.3	53.9	3.3	21.9	5.1	32.0	6.1
11–12	1	<MDA	-	47.0	7.3	30.4	4.4	16.6	8.5
12–13	1	<MDA	-	32.2	5.8	25.9	5.6	6.3	8.1
13–14	1	<MDA	-	30.1	4.7	25.9	5.5	4.2	7.2
14–15.5	1.5	<MDA	-	28.0	3.5	21.2	3.9	6.8	5.2
15.5–17.5	2	<MDA	-	34.6	2.5	25.5	3.9	9.1	4.6
17.5–19.5	2	<MDA	-	26.7	2.0	21.7	2.0	5.0	2.8
19.5–21.5	2	<MDA	-	32.9	3.2	31.1	3.0	1.8	4.4
21.5–23.5	2	<MDA	-	33.4	3.9	28.8	2.3	4.6	4.5
23.5–25.5	2	<MDA	-	28.6	3.0	23.7	2.7	4.9	4.0

[1] U—standard uncertainty.

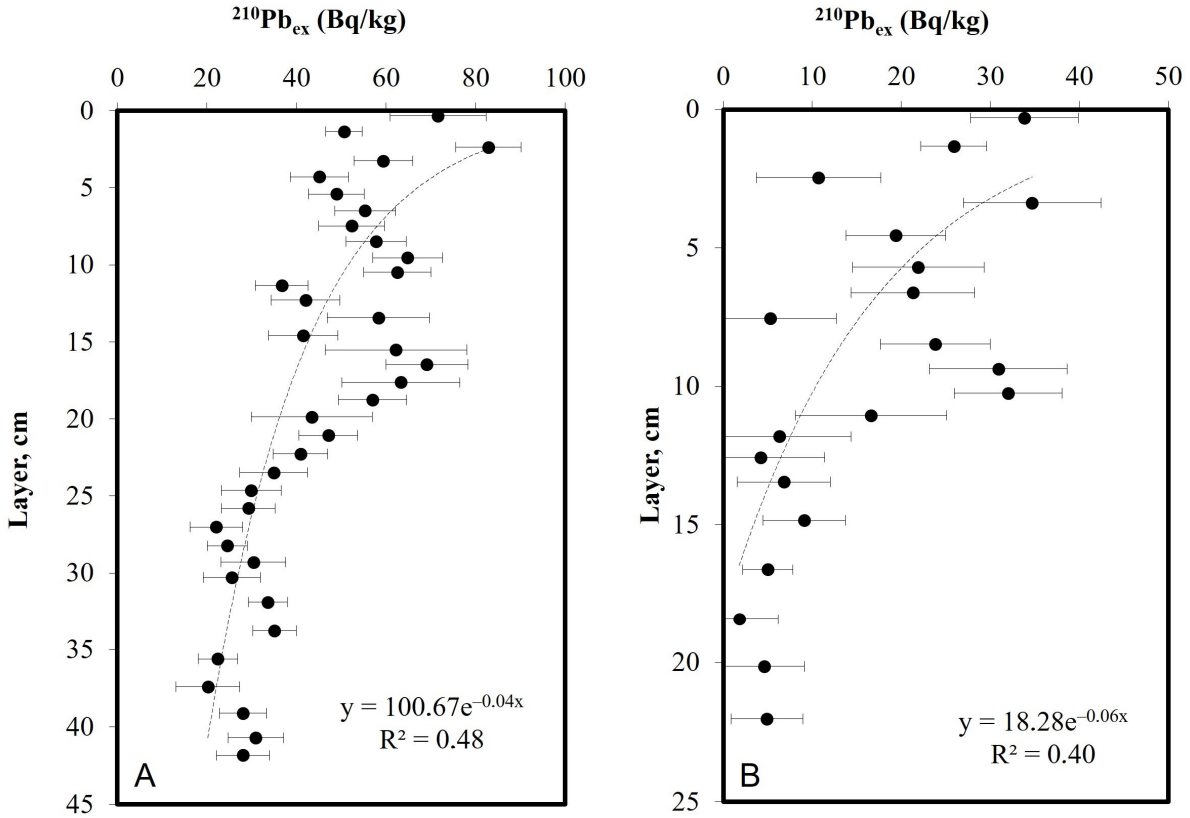

Figure 4. The distribution of excess ^{210}Pb in the sediment cores: (**A**) "ice scour" (ANS-52-16); (**B**) "background" (ANS-52-17).

4.4. The Calendar Age and the Sediment Accumulation Rates

The calendar age and the sediment accumulation rate (SAR) of each sedimentary layer top in the studied sediment cores were calculated using the CF model [49], based on the measurements of the excess ^{210}Pb activity (Figures 5 and 6, Tables S1 and S2 in Supplementary Materials). In the "ice scour" core, the calculations were based on the assumption that the equilibrium between ^{210}Pb and ^{226}Ra must be achieved in the underlying layers not penetrated by the corer, i.e., the supposed equilibrium border is at 43 cm (curve "Pb-210 age, ice scour, CF/43" in Figure 5). In the "background" core, the calculations were carried out taking into account the accepted equilibrium border at 19.5 cm (curve "Pb-210 age, background, CF/19.5" in Figure 5). The obtained calendar ages have the form of decimal fractions since they are calculated mathematically, relative to the date of the core selections—2 November 2021 (2021.8 AD).

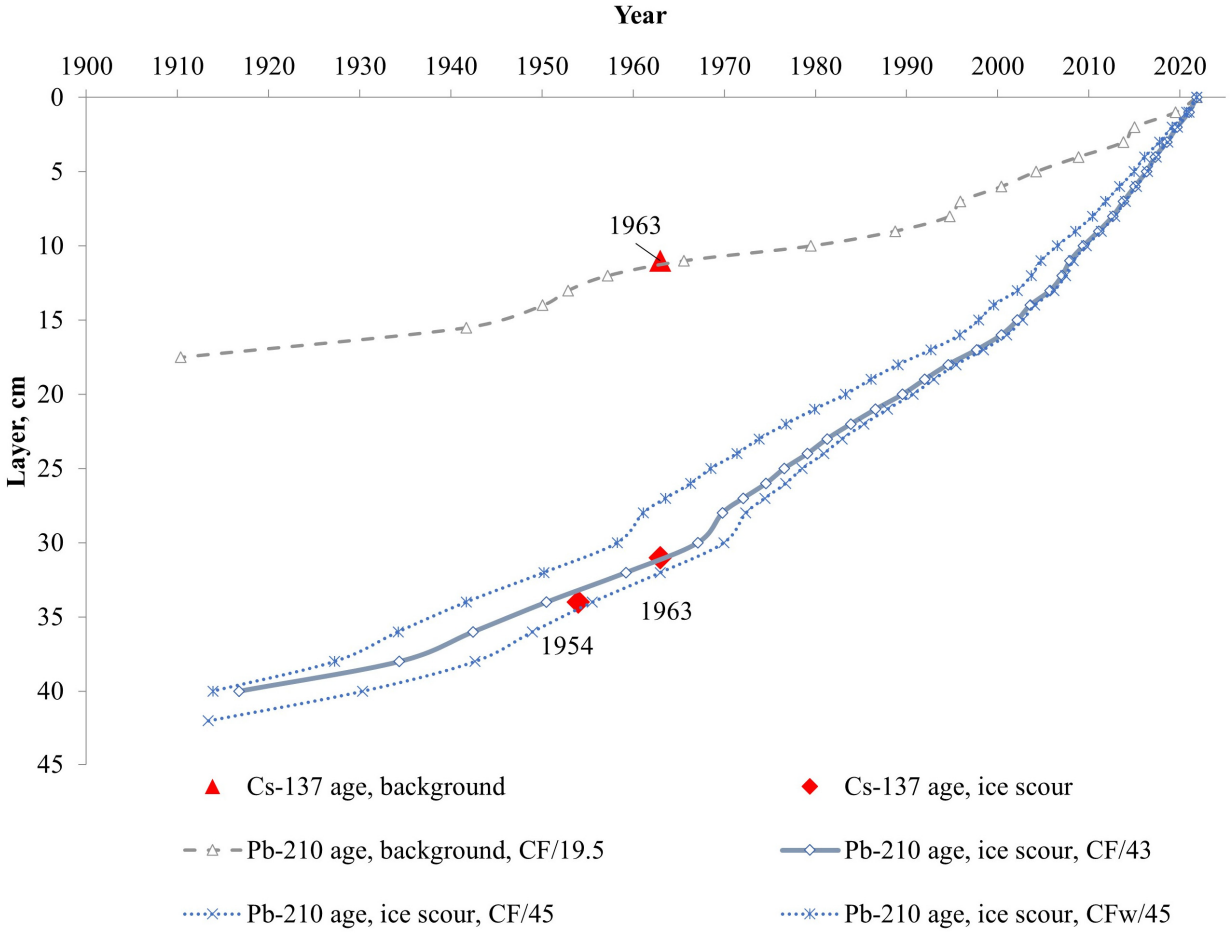

Figure 5. Distribution of the calendar ages of the layers by the depth of the cores ("ice scour" and "background"). Calendar ages are given according to ^{210}Pb and ^{137}Cs data. The designation "CF/43" contains the numerator information about the formulae used in the calculation (CF—constant flux model, CFw—modified formulae of the CF model, taking into account the change in the sedimentary layers' widths in the ice scour with depth), and the denominator contains information about the position of the equilibrium boundary, as used in the calculation (19.5; 43 and 45 cm).

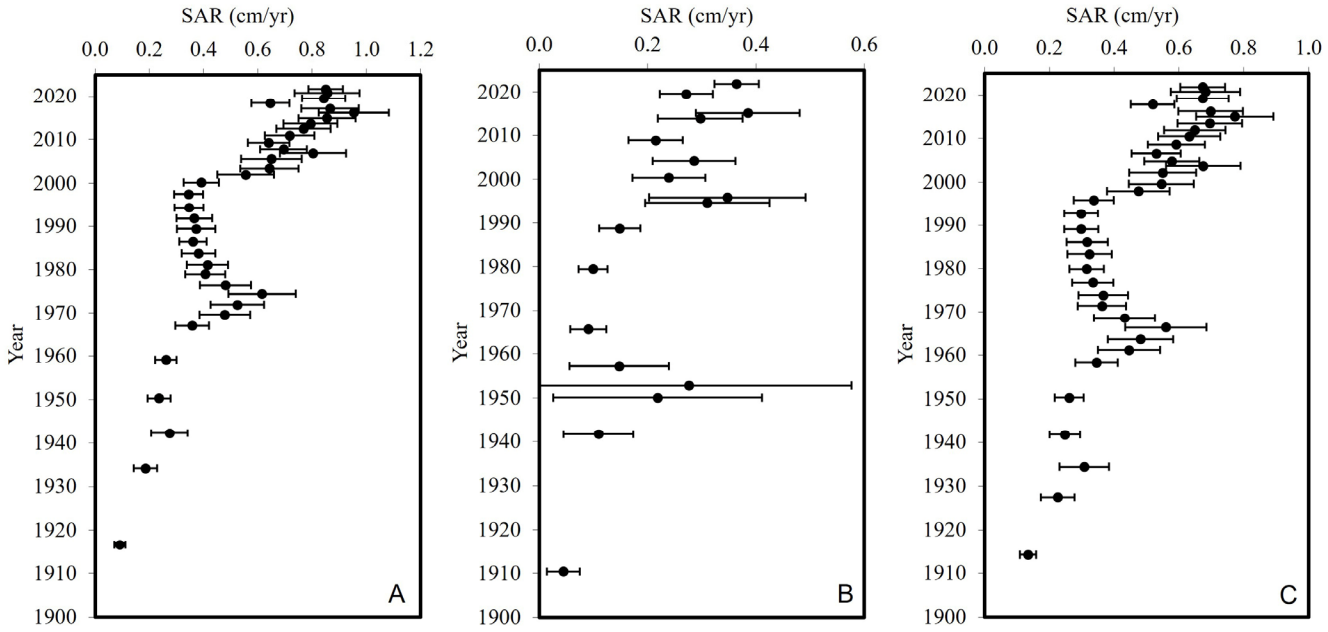

Figure 6. Changes in the sedimentation rate: (**A**) in the "ice scour" core (ANS-52-16) according to the CF model with the supposed equilibrium border at 43 cm (CF/43); (**B**) in the "background" core (ANS-52-17) according to the CF model with the accepted equilibrium border at 19.5 cm (CF/19.5); (**C**) in the "ice scour" core (ANS-52-16) according to the modified formulae of the CF model, taking into account the change in the sedimentary layers' widths in the scour, with the estimated boundary at 45 cm (CFw/45).

The calendar age of the lowest reliably dated levels is 1916.8 ± 4.9 AD (40 cm) in the "ice scour" core and 1910.4 ± 17.9 AD (17.5 cm) in the "background" core (Figure 5, Tables S1 and S2 in Supplementary Materials). The age value of 1884.1 ± 7.0 AD per 42 cm in the "ice scour" core is not considered, as it is beyond the limits of the method capabilities. Thus, the upper 40 cm in the "ice scour" core accumulated over the last 105 ± 4.9 years and the upper 17.5 cm in the "background" core accumulated over the last 111.4 ± 17.9 years.

The SARs in the "ice scour" core varied within the range of 0.09–0.95 cm/year in different years (Figure 6A, Table S1 in Supplementary Materials). The average SAR value for a thickness of 40 cm was 0.38 cm/year. The SARs in the "background" core were lower (0.04–0.38 cm/year), with an average value for a thickness of 17.5 cm of 0.16 cm/year (Figure 6B, Table S2 in Supplementary Materials). Comparing the distribution of the calendar ages and SAR values in both of the cores (Figures 5 and 6), one can notice the same trends in the change of rates but they occur at different times. The increase in the sedimentation rates in the ice scour occurs 10–20 years later compared to the background surface. For example, in the "ice scour" core, a sharp SAR increase occurred between 2000 ± 1 and 2002 ± 1, and in the "background" core it was between 1989 ± 4 and 1995 ± 3.

5. Discussion

5.1. Estimation of Missing Inventory of ^{210}Pb in the Ice Scour

Since there is no ^{210}Pb equilibrium with the initial radionuclide ^{226}Ra in the "ice scour" core, we estimated the missing inventory of ^{210}Pb (A(j), Bq/m^2) in the layers below 43 cm, not penetrated by the corer. To do this, we used two methods: the formula of the exponential dependence of the total ^{210}Pb on the mass (m$_i$, g/cm^2) $y = 159.44e^{-0.035x}$ and ^{137}Cs time marker estimation [49].

Using the formula of the first method, the total ^{210}Pb was reconstructed in the range of 43–51 cm. The mass of the layers was taken from the average value of the layers in the range of 32–40 cm (21.26 g). ^{226}Ra was calculated as the average value of the specific activity

for all of the layers and amounted to 26.4 ± 7 Bq/kg. Subsequently, the calculation was carried out according to the CF model with discreteness of 2 cm. Equilibrium was reached on a layer of 50 cm, which dates back to 1806 AD, which cannot be taken as representative information, as it is beyond the limits of the method capabilities. However, the dates in the range of 0–40 cm did not change significantly.

As a time marker of the second method, we used the ^{137}Cs peak (47.3 ± 0.9 Bq/kg), which was found in the 30–32 cm layer. According to the results of our measurements (Table S1 in Supplementary Materials), the inventory of non-equilibrium ^{210}Pb (δA_1, Bq/m^2) that accumulated over 58 years from 1963 to 2021 (0–32 cm) was 15,341 Bq/m^2. The inventory of ^{210}Pb ($A(j)_1$ = 2915 Bq/m^2) that accumulated before 1963 (layers from 32 cm to the boundary of equilibrium between ^{210}Pb and ^{226}Ra) was calculated using the formula $A(j)_1 = \delta A_1/(e^{\lambda t} - 1)$, where t = 58 yr and λ = 0.03118 yr^{-1} (disintegration constant). Based on the obtained values, the total inventory of non-equilibrium ^{210}Pb from the seabed surface to the equilibrium boundary was 18,256 Bq/m^2 ($A(0) = \delta A_1 + A(j)_1$). According to the results of our measurements (Table S1 in Supplementary Materials), the inventory of non-equilibrium ^{210}Pb (δA_2, Bq/m^2) accumulated in the layers (0–43 cm) was 17,879.5 Bq/m^2. Then, the missing inventory of ^{210}Pb ($A(j)_2 = A(0) - \delta A_2$) is 376.5 Bq/m^2. Based on the activity of non-equilibrium ^{210}Pb in the 42–43 cm layer, which is equal to 244 Bq/m^2, it can be assumed that the missing inventory of 377 Bq/m^2 accumulated in the 43–45 cm layer. In this case, the equilibrium boundary should be lowered by 3 cm to 46 cm.

The results of the layers' age calculations using the CF model, taking into account the estimation of the underlying missing inventory (curve "Pb-210 age, ice scour, CF/46"), are shown in the graph (Figure 5). This calculation makes the age a little younger: for layers in the range of 0–26 cm—no more than 2 years, in the range of 26–36 cm—no more than 5 years and in the range of 36–40 cm—no more than 8.5 years. The greatest age change is observed for the 40–42 cm layer, whose age has become 13.5 years younger.

5.2. Application of the Constant Flux Model in the Ice Scour Conditions

The CF model was designed for flat bottom sedimentation without any lateral limitations [49]. However, the accumulation of sediments in an ice scour occurs in a constrained environment. The sedimentation area at the bottom of the ice scour increases with time. In other words, as the ice scour is filled with sediments, the width of the ice scour bottom increases. This phenomenon is expressed in the cross section of the ice scour as an increase in the "width" of the layers upwards. Therefore, we calculated how the layer "width" changes with a step of 1 cm in an ice scour with a geometry such as ours, in order to assess the possible error in the results obtained from this model.

Calculations were made for an ice scour with w_0/S = 15, where w_0—the ice scour width at the present bottom surface, and S—the thickness of the ice scour filling sediments (in our case, w_0 = 12 m and S = 0.8 m). This ratio shows the absolute value of the change in the ice scour width, which is constant and amounts to 15 cm per 1 cm. With this ratio, the angle of inclination of the ice scour sides is 7.6 degrees. The ice scour width at a given depth relative to the present bottom surface was calculated using the formula w_i = 12–15 z_i, where w_i is the ice scour width at a given horizon, and z_i is the depth of horizon. The 0–1 cm layer (the uppermost dated layer) will have a roof "width" of 12.0 m and a base "width" of 11.85 m. The change is 1.25%. In the 38–40 cm layer (the lowest dated layer), the "width" of the roof will be 6.3 m, and the "width" of the base will be 6.0 m. The change is 4.8%. There is a downward trend of increasing the magnitude of the layers' "width" relative changes which can reach 50–100% at the base of the filling sediments under the condition of an ideal cross section of the ice scour in the form of an isosceles triangle. However, we dated only the upper half of the filling sediments (40 cm out of 80 cm), where the "width" of 1 cm layers in the cross section changes by only 1.25–2.4% per 1 cm.

Such an insignificant change in the 1 cm layers' "width" in the cross section gives grounds in our case to neglect the influence of the ice scour geometry on sedimentation. Therefore, we consider it reasonable to use the CF model to calculate the age in both cores:

on the "background" surface, where the layers' "width" remains constant, and in 0–40 cm of the ice scour, where the layers' "width" changes no more than 2.4% per 1 cm. It is important to note that we realize that the results may have additional uncertainty, but it is not significant and does not exceed the standard uncertainty in the measurements themselves. The uncertainty increases with the increase in the thickness of the analyzed layers.

Another important fact is worth noting. As the ice scour fills with sediments, each successive layer becomes "wider". Therefore, at a constant sediment flux entering the ice scour, the sedimentation rate should decrease with time. However, we observe the opposite picture—the sedimentation rate increases with time. From this, it can be concluded that the sediment flux entering the ice scour has a greater effect on the sedimentation rate than the ice scour layers' "width", whose influence is insignificant.

An additional control of the reliability of the ice scour dating results can be undertaken by comparing them with the results of the "background" core dating. Due to the close location (only 140 m between the cores), the general tendencies of sedimentation in this bottom area should be traced in both of the cores, while the sedimentation rates can be determined according to local conditions (in our case, according to the features of the bottom topography). Indeed, in both cores, an exponential distribution of ^{210}Pb was observed, whereby the fluctuations (peaks) of which are correlated between the cores (Figure 4). However, there is a 10–20 year lag of the sharp SAR changes in the ice scour relative to the background surface (Figure 6), which may be due to uncertainty due to the layers' width changes in the ice scour.

To eliminate this uncertainty, an attempt was made to modify the formulae of the CF model to take into account the change with depth in the sedimentary layers' width in the scour. The calculation using these modified formulae was designated as CFw (Table S3 in Supplementary Materials). Whereas the CF model calculation is based on the measured specific activity of radionuclides in the core, the CFw calculation is based on an estimation of the excess lead activity in all of the sediments filling the ice scour. To extrapolate the excess lead activity that had accumulated over the entire cross section of the ice scour, the excess lead activity in each layer was multiplied by the proportionality factor (k_i) of the ice scour width at a given depth to the ice scour width at the lowest horizon with the excess lead activity. Thus, at the lowest horizon (44 cm), k_i is equal to 1, and at the highest horizon (the present surface of the bottom of the ice scour), k_i reaches a value of 2.22. It was decided that k_i be used, because it was noted that the results of the age and SAR calculations were affected by the rate of increase in values with each subsequent step in the horizon depth change, and not by the absolute values themselves, and by which, the excess lead activity in the core was multiplied. Thus, the calculation results were the same both when the excess lead activity was multiplied by the ice scour width at a given horizon depth, and when the excess lead activity was multiplied by the ratio of the ice scour width at a given horizon depth to the core diameter. The modified formulae used for the CFw calculation are presented in the Supplementary Materials.

The calendar age obtained from the CFw calculation turned out to be no more than 10 years earlier than the age obtained from the CF model (Figure 5, curve "Pb-210 age, ice scour, CFw/45″). Compared to the background surface, the lag of sharp changes in the SAR in the ice scour has decreased, but it still remains and has reached about 10 years (Figure 6C). This may be due to the lower detail and higher uncertainty in the "background" core compared to the "ice scour" core. The uncertainty in the calendar age calculation increases from the seabed surface down the core and reaches ±5 years in the ice scour and ±18 years on the background surface. Thus, the modified formulae (CFw) correct the age within the method uncertainty; so, this, together with what was noted above, gives us a reason to use the results obtained from the measured specific activities of radionuclides without taking into account the changing width of the ice scour (CF model) to estimate the ice scour age.

5.3. Verification of Results with ^{137}Cs

The lowest layer from the "ice scour" core, where ^{137}Cs was found (34–36 cm), can be attributed to 1954 AD (1950.5 ± 3.2 AD at 34 cm according to the CF model, Figure 5). This is the year when the first high-performance thermonuclear weapon was detonated and atmospheric levels of ^{137}Cs in the Northern Hemisphere rose high enough to create a measurable signal that could be detected in soils and sediments in water bodies [53]. The ^{137}Cs specific activity increased approximately 20 times in the overlying layer (30–32 cm). Seventy-five atmospheric nuclear tests were carried out on the Novaya Zemlya archipelago between 1954 and 1962, including the largest thermonuclear charge ever detonated ("Tsar Bomba") [54]. The global number of atmospheric nuclear tests peaked at 110 explosions in 1962 [55]. The peak concentration of atmospheric radioactivity was recorded in 1963 as a result of atmospheric nuclear testing [56]; so, the calendar age of the 30–32 cm layer should be attributed to this year, which is comparable to the chronological data obtained using the CF model (1967.1 ± 2.2 AD at 30 cm and 1959.2 ± 2.6 AD at 32 cm, Figure 5).

The further distribution of ^{137}Cs in the "ice scour" core from a layer 26–27 cm to the surface layer did not make it possible to identify the increased specific activity of the radionuclide designated as a reference in the literature, for example, the transoceanic transport of radioactive discharges of nuclear fuel reprocessing plant Sellafield, UK, to the Irish Sea (1982–1983) and atmospheric fallout after the accident at the Chernobyl Atomic Electric Power Station (1986) [57]. Thus, according to the ^{137}Cs data, the upper 34 cm in the "ice scour" core accumulated after 1954 AD over the last 67.8 years, and the average SAR value was 0.5 cm/year for a thickness of 34 cm, which is higher, but for a lower thickness than according to ^{210}Pb (0.38 cm/year for 40 cm).

The "background" core is characterized by low ^{137}Cs specific activity (<MDA), except for two layers (1–2 and 10–11 cm). This is probably due to periodic seabed erosion, which prevents the accumulation of ^{137}Cs in seabed sediments. The appearance of ^{137}Cs in the 10–11 cm layer allows us to interpret the calendar age of this layer as 1963 AD, which is comparable with the age obtained from ^{210}Pb (1965.6 ± 8.0 AD at 11 cm). Thus, according to the ^{137}Cs data, the upper 10 cm in the "background" core accumulated after 1963 AD over the last 58.8 years, and the average SAR value was 0.17 cm/year for a thickness of 10 cm, which is comparable to ^{210}Pb results (0.16 cm/year for 17.5 cm) even for a lower thickness.

5.4. Formation of Sediments and Dynamics of Their Accumulation

The "background" core is more than six times longer than the "ice scour" core. We explain the small length of the "ice scour" core by the presence of a compacted horizon, which is associated with the pressure during gouging. Probably, the corer did not hit the ice scour axis, but the lower part of the ice scour wall, which is covered by only 43 cm (or so) of filling post-gouging sediments. The GPS coordinates of the sampling point that were correlated with the DEM of the bottom also show the displacement of the sampling site toward the ice scour wall relative to its axis (Figure 2B). Thus, we have reason to believe that 43 cm of the sampled sediments lie on pre-exaration deposits. Older post-exaration deposits that fill the ice scour are located in the axial part of the ice scour at a depth of 43–80 cm below the modern bottom of the ice scour.

According to the grain size analysis (Tables 2 and 3), sediment accumulation in the ice scour and at the "background" surface occurs mainly due to fine sediments (pelite and silt). In the ice scour, in contrast to the "background" surface, there is an inclusion of heterogeneous sand and fine gravel, which accumulated here as a result of slope subaqueous processes, saltation or ice rafting. The low content of sand and gravel, as well as the lower natural moisture content in the sediments of the "background" surface, may indicate higher hydrodynamics outside of the ice scour. Since the studied sediment cores are located quite close to each other (only 140 m), the quantity and quality (grain size composition) of sedimentary material entered in the ice scour and on the "background" surface are the same; however, active hydrodynamics outside of the ice scour lead to periodic erosion of the "background" surface and to the removal of sand and gravel. Under conditions of

low hydrodynamics in the ice scour, coarse particles originating from ice rafting, slope processes and saltation are not able to move laterally and remain where they settled on the bottom. This fact explains the absence of the ^{137}Cs marker in the sediments of the "background" core and the availability of this isotope in high concentrations in the ice scour (Tables 4 and 5). In other words, the sediments that have accumulated into the ice scour are stored there as in a sedimentological trap and the sediments of the "background" surface pass in transit, only being partially deposited. Thus, the obtained results additionally confirm that one of the sediment cores was indeed taken directly from the ice scour.

To quantify the sedimentological trap effect, the excess lead activity accumulated on the present seabed surface in the "background" core was multiplied by the proportionality factor of the ice scour width at the level of the present seabed surface to the ice scour width at the lowest horizon with excess lead activity (k_0 = 2.22). The obtained value was 6684 Bq/m^2 on the background surface, while in the ice scour it was 31,497 Bq/m^2. Thus, the studied ice scour accumulated 4.7 times more lead than the background surface.

The main sources of fine sediments accumulated in Baydaratskaya Bay are the erosion of its coasts and partly the runoff of the Ust-Kara River (Figure 1). The northern coast of the bay is mainly composed of homogeneous sandy deposits with relatively low ice content [58,59] and is actively eroded at an average rate of 0.3 to 1.2 m/year [60]. The southern coast of the bay is composed of medium ice-rich sandy loam deposits, underlain by medium or, in some places, strongly ice-rich boulder loams and clays [61], and is also actively eroded at an average rate of 0.5 to 2.4 m/year [60]. Taking into account the grain size composition of the studied sediment cores, it can be assumed that sedimentation in the ice scour and near it occurs due to the erosion of the southern coast of Baydaratskaya Bay.

Sediments of the last 100–120 years and older are composed of the same grain size. Consequently, the source of sedimentation material (erosion products of the southern coast of the bay) and lithodynamics (secondary seabed erosion) have not changed in the studied area. Taking into account that sedimentation in the study area is closely related to coastal erosion, one can note a certain correlation between the coastal dynamics of Baydaratskaya Bay and the sedimentation rates in the studied sediment cores. According to our data (Figure 6), the SARs have reached their maximum values in recent years, since the 2000s. The maximum coastal erosion of the bay also belongs to the same period [60]. In the 1990s, when coastal erosion of the bay slowed down, we noted a decrease in the sedimentation rate. At the same time, it is known that the dynamics of coastal erosion are closely related to the climate and depend on combinations of wind–wave and thermal factors within the region [60]. Consequently, the rates of marine sedimentation also depend on the climate.

5.5. The Age of the Ice Scour

The ^{210}Pb method allowed us to date the upper part (0–0.4 m) of the sediments filling the ice scour, whereby thickness was estimated from seismic profiles to be about 0.6–0.8 m. We estimated the age of the ice scour for a filling sediment thickness of 0.7 m, assuming that age variations can occur both upwards and downwards due to variations in the actual thickness of the filling sediments. The age estimation of sediments in the range of 0.4–0.7 m is based on the extrapolation of the maximum and minimum possible mean sedimentation rates under certain sedimentation conditions.

It is known that marine sedimentation is determined by a few factors: climate, water salinity, basin depth, gas regime, the presence and nature of currents and biological activity [62]. At the same time, air temperature, as an important indicator of the climate, is a significant factor determining basin sedimentation. Often, there is a strong correlation between climatic components and sedimentation [63].

According to our calculations, the top 40 cm of sediment accumulated in the ice scour over about 105 $\pm$ 5 years, starting around 1917 $\pm$ 5 AD (mean SAR 0.38 cm/year). At the same time, more than 1/3 of the dated sediments (0–15 cm) accumulated over the past 20 $\pm$ 1 years (since around 2002 $\pm$ 1 AD) at a mean rate of about 0.75 cm/year. This period is characterized by an increase in air temperature in the Baydaratskaya Bay area, which

accelerated the processes of coastal erosion [64], increasing the sediment supply in the accumulation basin. Conversely, a decrease in the rate of sedimentation is observed with a decrease in the sum of daily positive air temperatures in the period of 1975–1985. In the 1960s, the dependence of sedimentation rates on air temperatures persisted. The sum of daily positive air temperatures increased and sedimentation proceeded more dynamically than in the next decade.

Thus, based on the past temperature regime, we can indirectly assume the mean sedimentation rate in the ice scour before 1917. Due to the lack of meteorological observations in the work area, we decided to rely on data on climatic anomalies of the northern hemisphere from 1850 to the present [65–67]. According to these data, the value of the temperature anomaly in 1900–1930 was unchanged. Considering this, it can be assumed that the mean SAR in the ice scour in that time was not less than the mean SAR established for the period 1916.8–1934.3 (38–40 cm), i.e., around 0.11 cm/year. In this case, in 1900–1916.8, a layer of 40–41.8 cm was formed; however, we found that a 42–43 cm layer contained excess ^{210}Pb. Therefore, its age cannot theoretically exceed 120 years (1901.8 AD) due to the dating limit of the method. Rounding the age of the beginning of the 42–43 cm layer formation to 1900 AD, it can be assumed that in 1900–1916.8, a layer of 40–43 cm was formed at a mean rate of 0.17 cm/year, rather than 40–41.8 cm. The values of temperature anomalies in 1850–1900 approximately corresponded to the temperature regime in 1930–1960. Therefore, we can assume that the mean SAR in the ice scour in 1850–1900 was not less than the mean SAR established for the period 1934.3–1959.2 (32–38 cm), i.e., around 0.24 cm/year. In this case, a layer of 43–55 cm was formed in 1850–1900. Thus, the mean sedimentation rate of the 15 cm stratum (40–55 cm) for 66.8 years (1850–1916.8) could be 0.22 cm/year. We consider this value as the minimum possible sedimentation rate before 1917. Considering that the warming since 2000 has been unprecedented, the mean rate of 0.38 cm/year determined for the thickness of 0–40 cm can be the maximum possible sedimentation rate for the period before 1917.

The extrapolation of the minimum (0.22 cm/year) and maximum (0.38 cm/year) possible sedimentation rates in the ice scour before 1917 allows us to estimate the time range at which the accumulation of the first sediments in the ice scour at a depth of 70 cm below the current seabed surface began. This time range is defined as 1780–1840. Thus, the age of the ice scour can be determined as 1810 $\pm$ 30 AD. The mean rate of ice scour filling with 70 cm thick sediments from the moment of its formation is around 0.33 cm/year.

6. Conclusions

- The studied ice scour, located in front of the entrance to Baydaratskaya Bay of the Kara Sea at a sea depth of about 28–32 m, has a serpentine-shaped plan configuration, changing its direction 2–3 times and reaching a length of at least 30–35 km. The maximum visible depth reaches 3.2 m, and the maximum width is up to 35 m. At present, it is the largest ice scour among those known in this region of the Kara Sea.
- Two sediment cores were studied, which were taken on 2 November 2021 (2021.8 A.D.) using a gravity corer directly in the ice scour and on the "background" seabed surface, which was not processed via ice scouring, and 140 m south of the first one. At the core sampling site, the apparent depth of the ice scour cutting into the background seabed surface was about 2.4 m. According to the seismic profiles, the thickness of sediments filling the ice scour was estimated at about 0.6–0.8 m, whereby the top 30 cm of which was presented exclusively by clayey silt. The pelite content varied from 52.9 to 68.4%, the silt content varied from 23.4 to 29.5% and the heterogeneous sand content varied from 4.2 to 16.4%. Some layers contained gravel grains. The highest content of fine gravel inclusions occurred in the upper part of the core. On the "background" seabed surface, the upper 50 cm of sediments was also represented by clayey silt. The pelite content varied from 56.6 to 72.7%, the silt content varied from 27.1 to 39.4% and the inclusion of heterogeneous sand and gravel was not significant. The low content of the sand and gravel in the sediments of the background surface is explained by

higher hydrodynamics outside of the ice scour, which leads to the periodic erosion of sediments and the removal of rare sand and gravel particles.

- The excess ^{210}Pb was found in all of the analyzed layers (up to 43 cm) of the ice scour sediments, reaching maximum values of specific activity (108 Bq/kg) in the upper horizons and decreasing to 48–55.9 Bq/kg toward the lower ones. The equilibrium of ^{210}Pb with the initial radionuclide ^{226}Ra was not revealed at the layer of 42–43 cm, but there was a tendency to approach it. The technogenic radionuclide ^{137}Cs below 36 cm was not detected, while above its content it ranged from 47.3 Bq/kg to values less than the minimum detectable activity (<0.2 Bq/kg).
- In deposits on the "background" seabed surface, the excess ^{210}Pb was only found in the upper 25.5 cm. Its specific activity decreased from top to bottom from 60 Bq/kg to 26.7 Bq/kg. The equilibrium of ^{210}Pb with the initial radionuclide ^{226}Ra was observed in the layer of 19.5–21.5 cm. The ^{137}Cs specific activity was below 0.2 Bq/kg at all horizons, except for the 1–2 cm and 10–11 cm layers. The low content of the technogenic radionuclide ^{137}Cs also indicates the periodic erosion of sediments.
- Based on ^{210}Pb dating, the time of the beginning of sediment accumulation in the ice scour at a depth of 15 cm was estimated to be around 2002 AD; at a depth of 38 cm—around 1934 AD; at a depth of 40 cm—around 1917 AD and at a depth of 43 cm—around 1900 AD. Thus, over the past 120 years, there has been an increase in the mean SARs: 0.79 cm/year for the 0–15 cm horizon, 0.43 cm/year for the 0–38 cm horizon, 0.38 cm/year for the 0–40 cm thickness and not less than 0.35 cm/year for the 0–43 cm horizon.
- On the "background" seabed surface outside of the ice scour, the mean sedimentation rate over the past 110 years has been two times lower. The time of the beginning of sediment accumulation outside of the ice scour at a depth of 17.5 cm is estimated to be around 1910 AD (0.16 cm/year). Fluctuations in the mean SARs are not pronounced, which may be due to the periodic erosion of sediments outside of the ice scour.
- There is a close correlation between the marine sedimentation rates and air temperature fluctuations, as well as the coastal retreat rates of Baydaratskaya Bay, whereby the erosion products of which are the main source of seabed sediments due to the absence of large rivers in the area. Thus, since 2002, in the Baydaratskaya Bay area, there has been a sharp increase in air temperature, the rate of coastal retreat and the rate of sedimentation in the largest ice scour of this region.
- According to the results of ^{210}Pb dating, the studied ice scour was formed no later than the end of the Little Ice Age (LIA) in the Arctic (turn of the 19th and 20th centuries). The age of the ice scour is estimated to be 1810 $\pm$ 30 AD based on the extrapolation of possible sedimentation rates prior to 1917 (0.22–0.38 cm/year). The mean rate of ice scour filling with 70 cm thick sediments from the moment of its formation is around 0.33 cm/year. Assuming that after the end of the LIA, the size of icebergs decreased, their penetration into Baydaratskaya Bay improved. Therefore, the ice scours of Baydaratskaya Bay were probably formed mainly after the end of the LIA, i.e., in the 20th century.
- Further study of the sedimentation chronology in ice scours will help to establish the periods of active ice scouring on the glaciated continental margins and to supplement knowledge about sedimentation on the Arctic shelf.

Supplementary Materials: The following supporting information can be downloaded at https://www.mdpi.com/article/10.3390/jmse11071404/s1: Table S1: Calculation of the sedimentary layers age (Year) and sedimentation rate (s(i)) in the "ice scour" core (ANS-52-16) using CF model (CF/43); Table S2: Calculation of the sedimentary layers age (Year) and sedimentation rate (s(i)) in the "background" core (ANS-52-17) using CF model (CF/19.5); Table S3: Calculation of the sedimentary layers age (Year') and sedimentation rate (s'(i)) in the "ice scour" core (ANS-52-16) using modified formulas of CF model (CFw/45).

Author Contributions: Conceptualization, O.K. and N.M.; methodology, O.K., I.U. and N.M.; field work, R.A., V.A., S.M. and N.S.; data analysis, O.K., I.U., N.M., R.A., V.A. and A.K.; writing—original draft preparation, O.K., I.U., N.M. and A.K.; writing—review and editing, O.K., A.K. and S.N. All authors have read and agreed to the published version of the manuscript.

Funding: The work was funded by the Russian Science Foundation, project no. 21-77-20038, GIN RAS, https://rscf.ru/en/project/21-77-20038/ (accessed on 10 July 2023). Dating results verification using Cs-137 was carried out within the framework of the MMBI RAS state assignment, topic no. 121091600105-4 (FMEE-2021-0029). Seismic profiling of previous cruises was obtained within the framework of the IO RAS state assignment, topic no. FMWE-2021-0005. A review of previous studies of the Baydaratskaya Bay ice scours was carried out within the framework of the MSU state assignment, topic no. 121051100167-1.

Institutional Review Board Statement: Not applicable.

Informed Consent Statement: Not applicable.

Data Availability Statement: Data available upon request from the authors.

Acknowledgments: We acknowledge the cruise administration, crew and participants of the R/V *Akademik Nikolaj Strakhov* (IO RAS) for their support and assistance in organizing the offshore activities and in obtaining and processing field data during the cruise. We are grateful to everyone who helped us greatly to improve the manuscript, and especially to the three reviewers, the JMSE issue editors for their helpful comments and Mitch Vowles for polishing our English.

Conflicts of Interest: The authors declare no conflict of interest.

References

1. Lewis, C.F.M. Estimation of the frequency and magnitude of drift-ice groundings from the ice scour tracks in the Canadian Beaufort Sea. In Proceedings of the 4th International Conference on Port and Ocean Engineering under Arctic Conditions, St. John's, NL, Canada, 26–30 September 1977; Volume 1, pp. 568–579.
2. Barnes, P.W.; Rearic, D.M.; Reimnitz, E. Ice gouging characteristics and processes. In *The Alaskan Beaufort Sea: Ecosystems and Environments*; Barnes, P.W., Schell, D.M., Reimnitz, E., Eds.; Academic Press Inc.: Orlando, FL, USA, 1984; pp. 185–212.
3. Woodworth-Lynas, C.M.T. The Geology of Ice Scour. Ph.D. Thesis, The University of Wales, Cardiff, UK, November 1992.
4. Dowdeswell, J.A.; Villinger, H.; Whittington, R.J.; Marienfeld, P. Iceberg scouring in Scoresby Sund and on the East Greenland continental shelf. *Mar. Geol.* **1993**, *111*, 37–53. [CrossRef]
5. Ogorodov, S.; Arkhipov, V.; Kokin, O.; Marchenko, A.; Overduin, P.; Forbes, D. Ice Effect on Coast and Seabed in Baydaratskaya Bay, Kara Sea. *Geogr. Environ. Sustain.* **2013**, *6*, 21–37. [CrossRef]
6. Brown, C.S.; Newton, A.M.W.; Huuse, M.; Buckley, F. Iceberg scours, pits, and pockmarks in the North Falkland Basin. *Mar. Geol.* **2017**, *386*, 140–152. [CrossRef]
7. Ananiev, R.; Dmitrevskiy, N.; Jakobsson, M.; Lobkovsky, L.; Nikiforov, S.; Roslyakov, A.; Semiletov, I. Sea-ice ploughmarks in the eastern Laptev Sea, East Siberian Arctic shelf. In *Atlas of Submarine Glacial Landforms: Modern, Quaternary and Ancient*; Dowdeswell, J.A., Canals, M., Jakobsson, M., Todd, B.J., Dowdeswell, E.K., Hogan, K.A., Eds.; Geological Society: London, UK, 2016; pp. 301–302. [CrossRef]
8. Mironyuk, S.G.; Ivanova, A.A.; Kolyubakin, A.A. Extreme depths of modern ice gouging on the shelf of the northeastern part of the Barents Sea. *Ross. Polyarn. Issled.* **2018**, *1*, 12–14.
9. Maznev, S.; Ogorodov, S.; Baranskaya, A.; Vergun, A.; Arkhipov, V.; Bukharitsin, P. Ice-Gouging Topography of the Exposed Aral Sea Bed. *Remote Sens.* **2019**, *11*, 113. [CrossRef]
10. Bogoyavlensky, V.I.; Kishankov, A.V.; Kazanin, A.G. Heterogeneities in the Upper Part of the Section of the East Siberian Sea Sedimentary Cover: Gas Accumulations and Signs of Ice Gouging. *Dokl. Earth Sc.* **2022**, *505*, 411–415. [CrossRef]
11. Ottesen, D.; Dowdeswell, J.A. Distinctive iceberg ploughmarks on the mid-Norwegian margin: Tidally influenced chains of pits with implications for iceberg drift. *Arct. Antarct. Alp. Res.* **2022**, *54*, 163–175. [CrossRef]
12. Sokolov, S.Y.; Mazarovich, A.O.; Zakharov, V.G.; Zarayskaya, Y.A. Deep-Water Glacial Plow Marks in the Western Margin of the Barents Sea. *Dokl. Earth Sc.* **2022**, *503*, 75–80. [CrossRef]
13. Crane, K.; Vogt, P.R.; Sundvor, E. Deep Pleistocene Iceberg Plowmarks on the Yermak Plateau. In *Glaciated Continental Margins*; Springer: Dordrecht, The Netherlands, 1997; pp. 140–141. [CrossRef]
14. Arndt, J.E.; Niessen, F.; Jokat, W.; Dorschel, B. Deep Water Paleo-iceberg Scouring on Top of Hovgaard Ridge—Arctic Ocean. *Geophys. Res. Lett.* **2014**, *41*, 5068–5074. [CrossRef]
15. Condron, A.; Hill, J.C. Timing of iceberg scours and massive ice-rafting events in the subtropical North Atlantic. *Nat. Commun.* **2021**, *12*, 3668. [CrossRef]

16. Barnes, P.W.; Rearic, D.M. Rates of sediment disruption by sea ice as determined from characteristics of dated ice gouges created since 1975 on the inner shelf of the Beaufort Sea, Alaska. In *Open-File Report 85-463*; U.S. Geological Survey: Reston, VA, USA, 1985; pp. 1–35. [CrossRef]
17. Ogorodov, S.A.; Arkhipov, V.V.; Baranskaya, A.V.; Kokin, O.V.; Romanov, A.O. The Influence of Climate Change on the Intensity of Ice Gouging of the Bottom by Hummocky Formations. *Dokl. Earth Sci.* **2018**, *478*, 228–231. [CrossRef]
18. Aliyev, R.; Kalmykov, S. *Radioactivity: Tutorial*; Lan: St. Petersburg, Russia, 2013; 304p. (In Russian)
19. *Environmental Conditions of the Baydaratskaya Bay: The Main Results of Investigations for the Construction of the Yamal-Center Submarin Gas Pipeline System Crossing*; Baulin, V.V.; Dubikov, G.I.; Komarov, I.A.; Koreysha, M.M.; Parmuzin, S.Y.; Sovershaev, V.A.; Tuzhilkin, V.S. (Eds.) GEOS: Moscow, Russia, 1997; 432p. (In Russian)
20. *Ice Feartures of the Western Arctic Seas*; Zubakin, E.K. (Ed.) AANII: St. Petersburg, Russia, 2006; 272p. (In Russian)
21. Maznev, S.V.; Kokin, O.V.; Arkhipov, V.V.; Baranskaya, A.V. Modern and Relict Evidence of Iceberg Scouring at the Bottom of the Barents and Kara Seas. *Oceanology* **2023**, *63*, 84–94. [CrossRef]
22. Ogorodov, S.A.; Arkhipov, V.V.; Kokin, O.V. Climate Change Effect on the Intensity of Seabed Gouging by Hummocky Ice Floes. In *Arctic, Subarctic: Mosaic, Contrast, Variability of the Cryosphere: Proceedings of the International Conference*; Melnikov, V.P., Drozdov, D.S., Eds.; Epoha Publishing House: Tyumen, Russia, 2015; pp. 269–271. (In Russian)
23. Biryukov, V.Y.; Sovershaev, V.A. The relief of the bottom of the southwestern part of the Kara Sea and the history of its development in the Holocene. In *Geology and Geomorphology of Shelves and Continental Slopes*; Nauka: Moscow, Russia, 1985; pp. 89–95. (In Russian)
24. Ogorodov, S.A. *The Role of Sea Ice in Coastal Dynamics*; Moscow University Press: Moscow, Russia, 2011; 173p. (In Russian)
25. Ogorodov, S.A.; Arkhipov, V.V.; Kokin, O.V.; Marchenko, A.V. Comprehensive Monitoring of Ice Gouging Bottom Relief at Key Sites of Oil and Gas Development within the Coastal-Shelf Zone of the Yamal Peninsula, Kara Sea. In Proceedings of the International Conference on Port and Ocean Engineering under Arctic Conditions, POAC, Busan, Republic of Korea, 11–16 June 2017; pp. 123:1–123:12.
26. Arkhipov, V.V.; Kokin, O.V.; Ogorodov, S.A.; Godetyskiy, S.V.; Tsvetsinskiy, A.S.; Onishchenko, D.A. The Yamal coast fast ice edge of the Baidaratskaya Bay of the Kara Sea in 2012–2016: Dynamics and role in formation of modern ice gouges on the sea-bed. *Vesti Gazov. Nauk.* **2017**, *4*, 129–136. (In Russian)
27. Gurevich, V.I. *Modern Sedimentogenesis and Geoecology of the Western Arctic Shelf of Eurasia*; Nauchnyy Mir: Moscow, Russia, 2002; 135p. (In Russian)
28. Polyak, L.; Levitan, M.; Khusid, T.; Merklin, L.; Mukhina, V. Variations in the influence of riverine discharge on the Kara Sea during the last deglaciation and the Holocene. *Global Planet. Chang.* **2002**, *32*, 291–309. [CrossRef]
29. Stein, R.; Dittmers, K.; Niessen, F.; Fahl, K. Siberian river run-off and Late Quaternary glaciation in the southern Kara Sea, Arctic Ocean: Preliminary results. *Rep. Polar Mar. Res.* **2002**, *21*, 315–322. [CrossRef]
30. Galimov, E.M.; Kodina, L.A.; Stepanets, O.V.; Korobeinik, G.S. Biogeochemistry of the Russian Arctic. Kara Sea: Research Results under the SIRRO Project, 1995–2003. *Geochem. Int.* **2006**, *44*, 1139–1191. [CrossRef]
31. Stepanets, O.; Borisov, A.; Ligaev, A.; Galimov, E. The investigation of sedimentation rate of the Kara Sea modern sediments using radioactive tracer. *Rep. Polar Mar. Res.* **2001**, *393*, 205–212.
32. Stepanets, O.V.; Borisov, A.P.; Travkina, A.V.; Soloveva, G.Y.; Vladimirov, M.V.; Aliev, R.A. Application of the ^{210}Pb and ^{137}Cs radionuclides in the geochronology of modern sediments at the storage sites of solid radioactive wastes in the Arctic Basin. *Geochem. Int.* **2010**, *48*, 398–402. [CrossRef]
33. Rusakov, V.Y.; Borisov, A.P.; Solovieva, G.Y. Sedimentation rates in different facies–genetic types of bottom sediments in the Kara Sea: Evidence from the ^{210}Pb and ^{137}Cs radionuclides. *Geochem. Int.* **2019**, *57*, 1185–1200. [CrossRef]
34. Nikiforov, S.L.; Sorokhtin, N.O.; Ananiev, R.A.; Dmitrevskiy, N.N.; Moroz, E.A.; Kokin, O.V. Research in Barents and Kara Seas during cruise 52 of the R/V Akademik Nikolaj Strakhov. *Oceanology* **2022**, *62*, 433–434. [CrossRef]
35. Andreeva, I.A.; Lapina, N.N. *Method of Grain-Size Analysis of Bottom Sediments of the World Ocean and Geological Interpretation of the Results of Laboratory Study*; VNIIOkeangeologia: St. Petersburg, Russia, 1998. (In Russian)
36. Klenova, M.V. *Geology of the Seas*; Uchpedgiz: Moscow, Russia, 1948; 495p. (In Russian)
37. Appleby, P.G.; Nolan, P.J.; Gifford, D.W.; Godfrey, M.J.; Oldfield, F.; Anderson, N.J.; Battarbee, R.W. 210 Pb dating by low-background gamma. *Hydrobiologia* **1986**, *143*, 21–27. [CrossRef]
38. Schelske, C.L.; Peplow, A.; Brenner, M.; Spencer, C.N. Low-background gamma counting: Applications for 210 Pb dating of sediments. *J. Paleolimnol.* **1994**, *10*, 115–128. [CrossRef]
39. Appleby, P.G.; Piliposian, G.T. Efficiency corrections for variable sample height in well-type germanium gamma detectors. *Nucl. Instrum. Methods Phys. Res. Sect. B Beam Interact. Mater. At.* **2004**, *225*, 423–433. [CrossRef]
40. Aliev, R.A.; Bobrov, V.A.; Kalmykov, S.N.; Melgunov, M.S.; Vlasova, I.E.; Shevchenko, V.P.; Novigatsky, A.N.; Lisitzin, A.P. Natural and artificial radionuclides as a tool for sedimentation studies in the Arctic region. *J. Radioanal. Nucl. Chem.* **2007**, *274*, 315–321. [CrossRef]
41. Zaborska, A.; Carroll, J.; Papucci, C.; Torricelli, L.; Carroll, M.L.; Walkusz-Miotk, J.; Pempkowiak, J. Recent sediment accumulation rates for the Western margin of the Barents Sea. *Deep.-Sea Res.* **2008**, *55*, 2352–2360. [CrossRef]
42. Kuzyk, Z.; Gobeil, C.; Macdonald, R. ^{210}Pb and ^{137}Cs in margin sediments of the Arctic Ocean: Controls on boundary scavenging. *Glob. Biogeochem. Cycles* **2013**, *27*, 422–439. [CrossRef]

43. Goryachenkova, T.A.; Borisov, A.P.; Solov'eva, G.Y.; Lavrinovich, E.A.; Kazinskaya, I.E.; Ligaev, A.N.; Travkina, A.V.; Novikov, A.P. Content of Technogenic Radionuclides in Water, Bottom Sediments, and Benthos of the Kara Sea and Shallow Bays of the Novaya Zemlya Archipelago. *Geochem. Int.* **2019**, *57*, 1320–1326. [CrossRef]
44. Demina, L.; Dara, O.; Aliev, R.; Alekseeva, T.; Budko, D.; Novichkova, E.; Politova, N.; Solomatina, A.; Bulokhov, A. Elemental and Mineral Composition of the Barents Sea Recent and Late Pleistocene−Holocene Sediments: A Correlation with Environmental Conditions. *Minerals* **2020**, *10*, 593. [CrossRef]
45. Robbins, J.A.; Edgington, D.N. Determination of recent sedimentation rates in Lake Michigan using Pb-210 and Cs-137. *Geochim. Cosmochim. Acta* **1975**, *39*, 285–304. [CrossRef]
46. von Gunten, H.R.; Moser, R.N. How reliable is the ^{210}Pb dating method? Old and new results from Switzerland. *J. Paleolimnotogy* **1993**, *9*, 161–178. [CrossRef]
47. Kirchner, G. ^{210}Pb as a tool for establishing sediment chronologies: Examples of potentials and limitations of conventional dating models. *J. Environ. Radioact.* **2011**, *102*, 490–494. [CrossRef]
48. Pittauerova, D.; Hettwig, B.; Fischer, H.W. Pb-210 sediment chronology: Focused on supported lead. *Radioprotection* **2011**, *46*, S277–S282. [CrossRef]
49. Sanchez-Cabeza, J.A.; Ruiz-Fernández, A.C. ^{210}Pb sediment radiochronology: An integrated formulation and classification of dating models. *Geochim. Cosmochim. Acta* **2012**, *82*, 183–200. [CrossRef]
50. Mabit, L.; Benmansour, M.; Abril, J.M.; Walling, D.E.; Meusburger, K.; Iurian, A.R. Fallout ^{210}Pb as a soil and sediment tracer in catchment sediment budget investigations: A review. *Earth-Sci. Rev.* **2014**, *138*, 335–351. [CrossRef]
51. Gharibreza, M.; Zaman, M.; Arabkhedri, M.S.-Z. The off-site implications of deforestation on sedimentation rates and pollution in Abkenar open water (Anzali Lagoon, Caspian Sea) using radionuclide techniques and sediment quality indices. *Int. J. Sediment Res.* **2021**, *37*, 370–382. [CrossRef]
52. Appleby, P.G. Chronostratigraphic techniques in recent sediments. In *Tracking Environmental Change Using Lake Sediments, Volume I: Basin Analysis, Coring, and Chronological Techniques*; Last, W.S., Smol, J.P., Eds.; Springer: Dordrecht, The Netherlands, 2002; pp. 171–203. [CrossRef]
53. Longmore, M.E. The caesium-137 dating technique and associated applications in Australiaea review. In *Archaeometry: An Australasian Perspective*; Ambrose, B.W., Duerden, P., Eds.; Australian National University Press: Canberra, Australia, 1982; pp. 310–321.
54. Khalturin, V.I.; Rautian, T.G.; Richards, P.G.; Leith, W.S. A Review of Nuclear Testing by the Soviet Union at Novaya Zemlya, 1955–1990. *Sci. Glob. Secur.* **2005**, *13*, 1–42. [CrossRef]
55. Norris, R.S.; Arkin, W.M. Known Nuclear Tests Worldwide, 1945–1994. *Bull. At. Sci.* **1995**, *51*, 70–71. [CrossRef]
56. Bergqvist, N.-O.; Ferm, R. *Nuclear Explosions 1945–1998 (FOA-R-00-01572-180)*; Defence Research Establishment: Stocholm, Sweden, 2000; 43p.
57. Kautsky, H. Determination of distribution processes, transport routes and transport times in the North Sea and the northern Atlantic using artificial radionuclides as tracers. In *Radionucludes: A Tool for Oceanography*; Guary, B.J.C., Guegueniat, P., Pentreath, R.J., Eds.; Elsevier Applied Science: London, UK, 1988; pp. 271–280.
58. Kamalov, A.M.; Ogorodov, S.A.; Birukov, V.Y.; Sovershaeva, G.D.; Tsvetsinsky, A.S.; Arkhipov, V.V.; Belova, N.G.; Noskov, A.I.; Solomatin, V.I. Coastal and seabed morpholithodynamics of the Baydaratskaya bay at the route of gas pipeline crossing. *Earth's Cryosphere* **2006**, *10*, 3–14. (In Russian)
59. Romanenko, F.A.; Garankina, E.V.; Shilova, O.S. Loose deposits stratigraphy and the formation of the relief of Western Yamal in the late Pleistocene–Holocene. In *Fundamental Problems of the Quarter: Results of the Study and the Main Directions of Further Research, Proceedings of the VI All-Russian Meeting of the Quaternary Period Research, Novosibirsk, Russia, 19–23 October 2009*; SO RAN: Novosibirsk, Russia, 2009; pp. 505–508. (In Russian)
60. Kopa-Ovdienko, N.V.; Ogorodov, S.A. Peculiarities of dynamics of thermoabrasional coasts of the Baydaratskaya Bay (Kara Sea) today. *Geomorfologiya* **2016**, *3*, 12–21. (In Russian) [CrossRef]
61. Romanenko, F.A.; Belova, N.G.; Nikolaev, V.I.; Olyunina, O.S. Features of the loose deposits structure of the Yugra coast of the Baydaratskaya Bay, the Kara Sea. In *Fundamental Problems of the Quarter: Results of the Study and the Main Directions of Further Research, Proceedings of the V All-Russian Meeting of the Quaternary Period Research, Moscow, Russia, 7–9 November 2007*; GEOS: Moscow, Russia, 2007; pp. 348–351. (In Russian)
62. Strakhov, N.M. *Types of Lithogenesis and Their Evolution in the History of the Earth*; Gosgeoltekhizdat: Moscow, Russia, 1963; 535p. (In Russian)
63. Meshcheryakov, N.I.; Usyagina, I.S.; Sharin, V.V.; Dauvalter, V.A.; Dukhno, G.N. Chronology of sedimentation in Colesbukta, Spitsbergen (Svalbard Archipelago): The results of the 2018 expedition. *IOP Conf. Ser. Earth Environ. Sci.* **2021**, *937*, 042081. [CrossRef]
64. Shabanova, N.; Ogorodov, S.; Shabanov, P.; Baranskaya, A. Hydrometeorological forcing of Western Russian arctic coastal dynamics: XX-century history and current state. *Geogr. Environ. Sustain.* **2018**, *11*, 113–129. [CrossRef]
65. Kennedy, J.J.; Rayner, N.A.; Atkinson, C.P.; Killick, R.E. An ensemble data set of sea surface temperature change from 1850: The Met Office Hadley Centre HadSST. *4.0.0.0 data set. J. Geophys. Res. Atmos.* **2019**, *124*, 7719–7763. [CrossRef]

66. Morice, C.P.; Kennedy, J.J.; Rayner, N.A.; Winn, J.P.; Hogan, E.; Killick, R.E. An updated assessment of near-surface temperature change from 1850: The HadCRUT5 data set. *J. Geophys. Res. Atmos.* **2021**, *126*, e2019JD032361. [CrossRef]
67. Osborn, T.J.; Jones, P.D.; Lister, D.H.; Morice, C.P.; Simpson, I.R.; Winn, J.P. Land surface air temperature variations across the globe updated to 2019: The CRUTEM5 data set. *J. Geophys. Res. Atmos.* **2021**, *126*, e2019JD032352. [CrossRef]

Disclaimer/Publisher's Note: The statements, opinions and data contained in all publications are solely those of the individual author(s) and contributor(s) and not of MDPI and/or the editor(s). MDPI and/or the editor(s) disclaim responsibility for any injury to people or property resulting from any ideas, methods, instructions or products referred to in the content.